
Article:
Caine, R.S. orcid.org/0000-0002-6480-218X, Khan, M.S. orcid.org/0000-0003-0506-5180, Brench, R.A. orcid.org/0000-0003-1900-4012 et al. (2 more authors) (2024) Inside-out: synergising leaf biochemical traits with stomatal-regulated water fluxes to enhance transpiration modelling during abiotic stress. Plant, Cell & Environment. ISSN 0140-7791

https://doi.org/10.1111/pce.14892

Received: 31 October 2023 | Revised: 17 February 2024 | Accepted: 8 March 2024

DOI: 10.1111/pce.14892

ORIGINAL ARTICLE

Plant, Cell & Environment | PC&E | WILEY

Inside-out: Synergising leaf biochemical traits with stomatal-regulated water fluxes to enhance transpiration modelling during abiotic stress

Robert S. Caine[1,2] | Muhammad S. Khan[1] | Robert A. Brench[1] | Heather J. Walker[1,2,3] | Holly L. Croft[1,2]

[1]Plants, Photosynthesis and Soil, School of Biosciences, University of Sheffield, South Yorkshire, UK

[2]School of Biosciences, Institute for Sustainable Food, University of Sheffield, South Yorkshire, UK

[3]biOMICS Mass Spectrometry Facility, School of Biosciences, University of Sheffield, South Yorkshire, UK

Correspondence
Robert S. Caine and Holly L. Croft, Plants, Photosynthesis and Soil, School of Biosciences, University of Sheffield, South Yorkshire S10 2TN, UK.
Email: b.caine@sheffield.ac.uk and h.croft@sheffield.ac.uk

Funding information
UK Research and Innovation (UKRI) Future Leaders Fellowship scheme, Grant/Award Number: MR/T01993X/1; The Institute of Sustainable Food at the University of Sheffield

Abstract

As the global climate continues to change, plants will increasingly experience abiotic stress(es). Stomata on leaf surfaces are the gatekeepers to plant interiors, regulating gaseous exchanges that are crucial for both photosynthesis and outward water release. To optimise future crop productivity, accurate modelling of how stomata govern plant–environment interactions will be crucial. Here, we synergise optical and thermal imaging data to improve modelled transpiration estimates during water and/or nutrient stress (where leaf N is reduced). By utilising hyperspectral data and partial least squares regression analysis of six plant traits and fluxes in wheat (*Triticum aestivum*), we develop a new spectral vegetation index; the Combined Nitrogen and Drought Index (CNDI), which can be used to detect both water stress and/or nitrogen deficiency. Upon full stomatal closure during drought, CNDI shows a strong relationship with leaf water content ($r^2 = 0.70$), with confounding changes in leaf biochemistry. By incorporating CNDI transformed with a sigmoid function into thermal-based transpiration modelling, we have increased the accuracy of modelling water fluxes during abiotic stress. These findings demonstrate the potential of using combined optical and thermal remote sensing-based modelling approaches to dynamically model water fluxes to improve both agricultural water usage and yields.

KEYWORDS
drought, evapotranspiration, hyperspectral, nitrogen, photosynthesis, remote sensing, stomata, thermal imaging

1 | INTRODUCTION

Agriculture is the largest consumer of freshwater, accounting for approximately 70% of the total global usage (Plett et al., 2020). As the human population continues to grow, demand for water is expected to outstrip supply in many regions, which could well be exacerbated by a changing climate and shifting temperature and precipitation regimes (López-Serrano et al., 2020). To protect future crop yields, optimisation of crop water-use and productivity will be critical, as will the implementation of targeted irrigation strategies (Bertolino et al., 2019;

Robert S. Caine and Muhammad S. Khan contributed equally to this study.

Hatfield & Dold, 2019). To regulate gaseous exchanges and to prevent desiccation, plants use finely tuneable pores called stomata, which are at the nexus of plant-environment interactions. By increasing pore aperture, stomata permit CO_2 to diffuse into plants for photosynthesis (*A*), and by reducing pore aperture, stomata also prevent excessive water loss (Buckley, 2019; Hatfield & Dold, 2019). Over longer durations, plants can further refine gaseous exchanges by altering stomatal size and stomatal density as new leaves develop (Bertolino et al., 2019; Franks & Beerling, 2009; Franks et al., 2012; Haworth et al., 2023). Transpiration (T), which is coupled with stomatal water release, allows the mass flow of water and nutrients from the soil to roots, and then up to shoots leading to plant growth and cooling (Matimati et al., 2014). Despite being frequently used to model water fluxes, measurements of modelled *T* over space and time are complicated, and models need to be enhanced if we are to optimise how future crops will use water. If predicting plant water-use can be improved, incidences of water-related plant stress will decrease leading to increases in productivity and ultimately yields.

Nitrogen (N) enhances plant *A*, T and yields (Mengel et al., 2006; Topcu et al., 2007). Such is its importance to agriculture, that global use of synthetic N-based fertilisers has increased ninefold, from 12 Tg N $year^{-1}$ in 1961 to 108 Tg N $year^{-1}$ in 2014 (Xu et al., 2020), contributing toward an approximate 250% increase in crop yields (Blomqvist et al., 2020). Within mature C3 leaves, N is invested within both photosynthetic and structural leaf components, where on average 75% of N is contained within chloroplasts (whereupon the majority is split between leaf chlorophyll, photosystem I and II, ATPase and RUBISCO), 10% in cell walls, 7.5% in cytosol, 5% in mitochondria and 2.5% in peroxisomes (Evans & Clarke, 2019). These respective allocations can differ according to environmental growth conditions and may change under plant stress. In a recent review of the literature, Mu and Chen (2021) highlight that under N stress, plants usually invest relatively more N in bioenergetics to maintain a high electron transport rate, and less N into photosynthetic enzymes and light harvesting proteins, which may act as N storage reservoirs. To optimise carbon capture and to maximise future crop yields, it is crucial that crops receive enough N to maximise productivity. It is also important to consider how the independent and combined interactions of N and water application affect crop physiology and productivity, due to N uptake being inherently linked with T, and T with N (Kunrath et al., 2020; Matimati et al., 2014; Shimshi, 1970).

Distinguishing N from water limitation can be difficult, particularly as water and N depletion often have combinatorial effects on plant phenotypes during abiotic stress (Araus et al., 2020; Yang et al., 2020). When water is limited in soils, stomatal closure leads to reductions in stomatal conductance to water vapour (g_{sw}), which reduces both *A* and T (Caine et al., 2019; Gerhards et al., 2016; Gupta et al., 2020; Shimshi, 1970). With continued drought, desiccation ensues, which impacts the efficiency at which the photosystems in the leaf can use light for photochemistry, and can be detected by changes in chlorophyll fluorescence (Caine et al., 2023; Woo et al., 2008). Over time, reductions in leaf chlorophyll content occur, which visually manifests as leaf yellowing as plants wilt, and leaf relative water content (RWC) drops (Yang et al., 2021). Like a drought stimulus, N deficiency also leads to reduced g_{sw} (and T), but in this case, stomatal closure is driven by a lower requirement for CO_2 due to a lower chlorophyll content (Mu & Chen, 2021). In the case of both drought and N deficiency, reduced g_{sw} causes leaf temperature rises, and it can be difficult to decipher which abiotic stress is driving the phenotypic response. Optical reflectance data from multispectral and/or hyperspectral sensors can be used to predict traits such as leaf chlorophyll, N, water content and plant gaseous exchanges (Cotrozzi et al., 2020; Croft et al., 2014; Curran et al., 1990; Mertens et al., 2021; Mohd Asaari et al., 2022; Yu, 2000), and this could hold the key for disentangling water stress from N stress when such data is combined with thermal imaging data. From remote sensing data, leaf N content is often derived via it's close relationship with leaf chlorophyll content, which has strong absorption in the visible spectrum, (Croft et al., 2017; Sage et al., 1987). N containing compounds (cellulose, lignin) also have absorption features in near infrared wavelengths (~1300–1600 nm); providing additional information for modelling N content. Water absorption features have been reported at 970, 1240, 1450, 1950, 2130 nm wavelengths (Caturegli et al., 2020).

Modelling changes in water fluxes and quantifying plant water-use permits a detailed understanding of crop water requirements over space and time. Dynamically modelling *T* and canopy conductance can be achieved through a surface energy balance approach (Jones et al., 2018; Page et al., 2018), which accounts for the sum of radiative energy received and lost by the leaf, and the mass transfer processes to the atmosphere (Zotarelli et al., 2010). The difficulty in obtaining longwave radiation measurements in agricultural field settings (Anderson & Kustas, 2008; Chen & Liu, 2020), has led to the use of thermal imaging, with the inclusion of dry references surfaces (DRS; Jones, 2002; Jones et al., 2018) to remove the need for radiation and humidity measurements (Vialet-Chabrand & Lawson, 2019). This method assumes that the DRS broadly imitates a nontranspiring leaf having similar emissivity and radiative properties to those of a plant canopy (Jones et al., 2018). However, there are caveats with current *T* models developed by combining the full energy balance of a DRS and the canopy. One limitation is a missing parameterization scheme for a range of crop water and nutrient stresses, which may cause uncertainties under different drought and/or fertilizer treatments due to changes in leaf emissivity. Optical-based remote sensing techniques have been shown to model both nutrient and water status of crops, which presents an opportunity to integrate optical-based leaf biochemistry trait data into thermal flux-based *T* modelling.

To investigate the individual and combined effects of water or nutrient stress on plant fluxes and traits, we develop an integrated approach, utilising the sensitivities to nutrient content and water fluxes from hyperspectral and thermal imaging data respectively. We combine a time-series of optical and thermal measurements with infrared gas analysis, porometry, and leaf area index (LAI) measurements across a nutrient and/or drought treatment, to address the following three questions: (1) Which technologies best detect early plant stress associated with drought or nutrient deficiency? (2) Can we develop a novel hyperspectral index that accurately describes the impact of multiple abiotic stresses on leaf water content? (3) Can we

combine hyperspectral and thermal imaging data to improve modelled *T* estimates for plants exposed to multiple abiotic stresses?

2 | MATERIALS AND METHODS

2.1 | Plant materials and growth conditions

To investigate plant responses to high N content nutrient fertiliser and/or water deficiency, we conducted a multiabiotic stress experiment on the elite British wheat (*Triticum aestivum L*) variety Mulika (Blackman Agriculture Ltd; Figure 1a). Seeds were sown on to 5:1 Levington M3:Perlite filled 0.8 l pots (IPP). Plants were grown continually at 15°C, with a 16 h:8 h, light:dark cycle with a photosynthetically active radiation (PAR) of 1000 µmol m^{-2} s^{-1} provided at canopy level. Relative humidity was set continually at 65% with CO_2 concentration at 450 ppm. A total of 128 plants were grown for 35 days with deionised water (dH_2O) applied to pot bases in trays when required. From Day 35, plants were divided into two subsets (64 plants each), where 64 plants were fed with soluble N-based fertiliser of 5 g of Chempak® High Nitrogen Feed—Formula 2 (Thompson and Morgan) dissolved in 2 L of dH_2O on a weekly basis until Day 60. The 64 plants receiving no additional high N fertiliser continued to receive DH_2O. From Days 60 to 83, fertilised and nonfertilised plants were divided into two further subsets with 32 plants from the fertiliser and DH_2O groups applied with drought, while 64 plants continued to receive DH_2O or soluble fertiliser. For both sets of droughted plants, tray water was removed at Day 60 and no subsequent water (or fertiliser) was added.

Field-grown wheat plants (variety Graham) were grown in North Grimston in North Yorkshire during the spring–summer season of 2021. N fertilised plants were supplied with 290 kg/ha in three equal splits during the growing season.

2.2 | Plant gas exchange

Stomatal conductance to water vapour (g_{sw}) was collected using a LI-600 porometer set to a flow of 150 µmol m^{-2} s^{-1} (LI-COR). Steady-state measurements were collected using LI-6800 Portable Photosynthesis Systems and attached Multiphase Flash Fluorometer (6800-01A) (LI-COR). Environmental conditions within the leaf chamber were set to light intensity = 1000 µmol m^{-2} s^{-1} PAR, 60% RH, T_{air} = 15°C, flow = 400 µmol s^{-1} and $[CO_2]_{ref}$ = 450 ppm. For each plant, 10 readings were taken under steady-state conditions over a 5-min period and averaged (n = 8 plants). To produce ACi curves to model photosynthetic traits, the same leaf chamber conditions were used, except T_{leaf} was set to 25°C, and light intensity set to 1800 µmol m^{-2} s^{-1} PAR. The $[CO_2]_{ref}$ sequence applied was: 450, 325, 200, 150, 100, 75, 50, 25, 450, 450, 450, 450, 600, 800, 1000, 1250, 1500, 1800 with a match conducted before each measurement with 2–4 min permitted between each $[CO_2]_{ref}$ treatment for stabilisation. The maximum carboxylation rate of rubisco (V_{cmax}) and the maximum rate of photosynthetic electron transport (J_{max}) were modelled using the Plantecophys package on R software (Duursma, 2015; R Team, 2021). Steady-state measurements were collected between Days 68 and 70 and Aci curve measurements between Days 76 and 77. For leaf stomatal analysis methodology see Caine et al. (2023). For all gas exchange measurements, the middle of the last fully expanded leaf was assessed.

2.3 | Thermal imaging

Thermal images of plants were captured using a FLIR T650sc thermal imaging camera. The central region of three fully expanded leaves from each plant were measured for each treatment for each time point, and were averaged to give an average leaf temperature per plant. Average leaf values were subtracted from the temperature of the green plastic hemispherical dry reference surface to calculate relative leaf temperature differences across the experiment. Images analysis was conducted in FLIR Researcher IR MAX (www.flir.co.uk) with heatmaps produced in Matlab (Mathworks).

2.4 | Hyperspectral data collection, analysis and vegetation index calculations

Leaf-level hyperspectral reflectance data (350–2500 nm) was collected using a PSR+ spectroradiometer (Spectral Evolution), with an attached Spectral Evolution leaf clip assembly equipped with a separate tungsten halogen illuminator light source. Target and reference panel measurements from a radiometrically calibrated 99% Spectralon panel were sampled sequentially. Data was imported into R via the Spectrolab package and to undertake partial least squares regression (PLSR) analysis, the Spectratrait package was used (Burnett et al., 2021a; Meireles et al., 2017). For all hyperspectral measurements, the middle of the last fully expanded leaf on the adaxial surface was assessed. The vegetation indices used in this study are set out in beneath.

Vegetation index name	Equations	References
MERIS Terrestrial Chlorophyll Index (MTCI)	$((R_{754} - R_{709})/(R_{754} - R_{709}))$	Dash and Curran (2007)
Normalised Difference Vegetation Index (NDVI)	$((R_{800} - R_{680})/(R_{800} + R_{680}))$	Banerjee et al. (2020)
Water Balance Index (WBI)	R_{970}/R_{900}	Peñuelas et al. (1993)
Water Potential Index 1 (WPI1)	$((R_{665} - R_{715})/R_{715})$	Mertens et al. (2021)
Relative water content	R_{1430}/R_{1850}	Yu (2000)
Combined Nitrogen and Drought Index (CNDI)	$R_{1353}/(R_{706} + R_{1402} + R_{1451} + R_{1878})$	Developed in this study

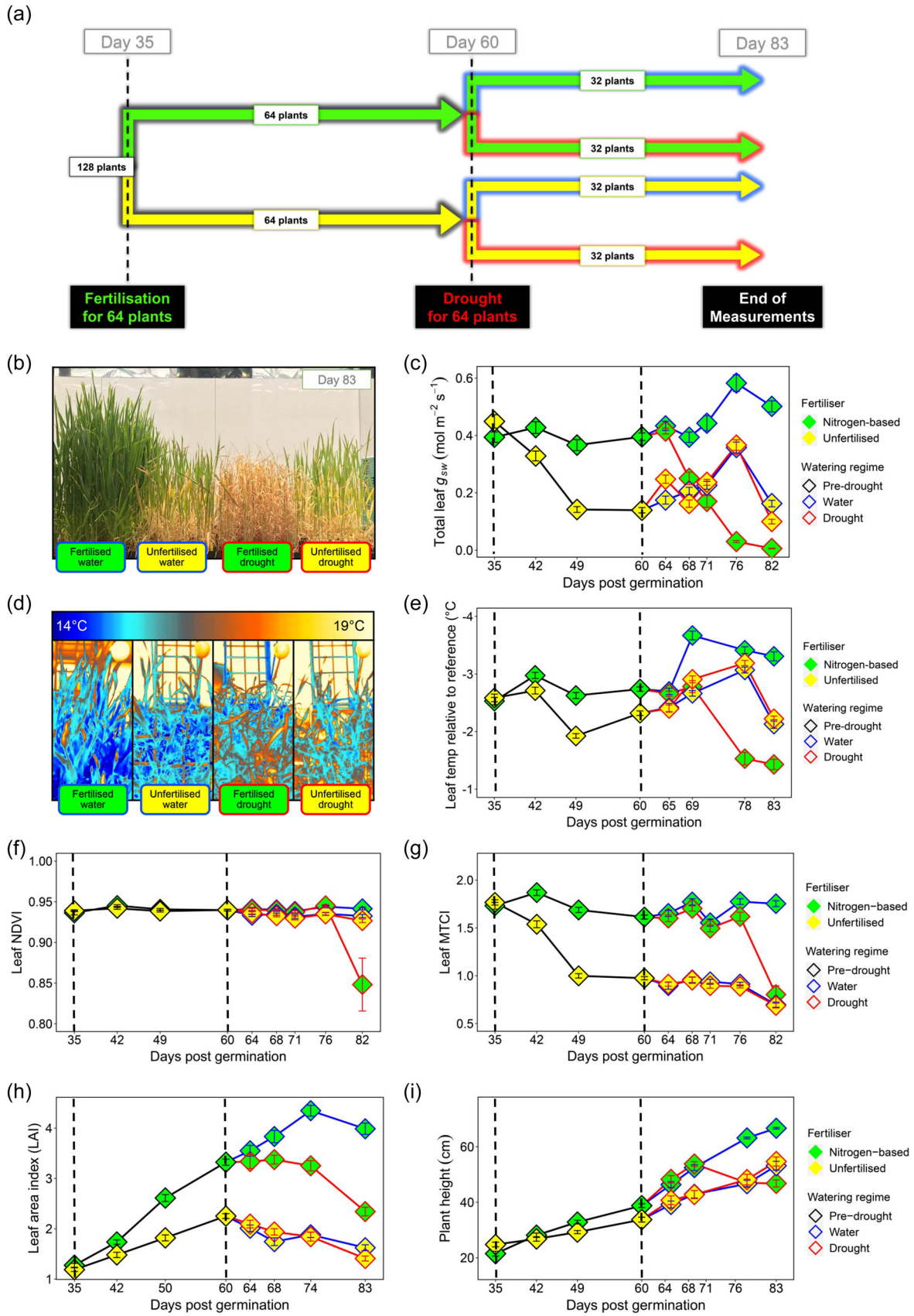

FIGURE 1 (See caption on next page).

2.5 | Leaf biochemical and canopy structural measurements

To sample leaf chlorophyll content, two leaf discs of 6 mm in diameter were weighed and placed into 5 mL of N,N-Dimethylformamide ≥99.8% ACS (Thermo scientific) and stored at 4°C for 3 days to enable chlorophyll extraction. Chlorophyll absorbance was measured at following wavelengths: 663.8, 646.8 and 480 nm (Wellburn, 1994), using a Shimadzu UV2600i spectrophotometer. To derive leaf water content (LWC), fresh leaf weight was measured and leaves were dried at 80°C for 7 days and weighed again to obtain dry weight. LWC was calculated by dividing the dry weight by the wet weight and then subtracting this value from 1 and subsequently multiplying by 100%. Isotope analysis of δ13C and % N content were obtained as in Field et al. (2016). For all leaf trait measurements, the area spanning the middle of the last fully expanded leaf was assessed. For each treatment of 32 plants, 24 measurements of LAI were collected using a LI-COR LAI-2200C Plant Canopy Analyzer.

2.6 | Transpiration modelling

For detailed formulations and step-by-step derivations of modelling transpiration (T) using the full energy balance-based equation, readers are directed to previous literature (Guilioni et al., 2008; Jones et al., 2018; Leinonen et al., 2006). A semi-empirical, full energy balance-based approach to modelling T can be achieved by integrating of a transpiring canopy (T_c) and a nontranspiring artificial DRS (T_{dry}) within the surface energy balance equation, by establishing a linear relationship between the T_{dry} and T_c temperature delta and T (Jones et al., 2018) as follows:

$$T = \rho C_p \alpha g_{HR}(T_{dry} - T_c). \quad (1)$$

T_{dry} and T_c are the DRS and leaf temperature respectively in unit Kelvin, ρ and C_p are the density and specific heat of air at the current temperature. The g_{HR} denotes the conductance to radiative transfer $g_R = \frac{4\sigma\varepsilon T_a^3}{\rho C_p}$ and boundary layer conductance to heat transfer (g_h) in series arrangement considering that conductance is the inverse of resistance (based on (Leinonen et al., (2006)). T_a is air temperature, ε is surface emissivity, and the Stefan–Boltzmann constant is represented with σ. To reduce uncertainties in modelled T due to erroneous spectral absorptance of the DRS, Jones et al. (2018) used a scaling coefficient (α), with a constant value of 0.5. To estimate g_H we implemented the formulations at the canopy scale (Monteith & Unsworth, 2013) as follows:

$$g_H = \frac{k^2 u_c}{[\log\left(\frac{h-d}{z_o}\right)]^2}, \quad (2)$$

$$u_c = u_{Ah} \times \frac{\log\left(\frac{h-d}{z_o}\right)}{\log\left(\frac{(Ah-d)}{z_o}\right)}, \quad (3)$$

where, k is von Karman's constant, h is canopy height, d is zero plane displacement height which is taken as 0.64*h, z_o is roughness height which is taken as 0.13*h, u_c is wind speed at the top of canopy, and u_{Ah} is wind speed at anemometer height (Ah) of 2 m in current study. To model g_H in this study, u_{Ah} was scaled to u_c by using the previous formulations to simulate T at canopy height (Jones, 2013; Monteith & Unsworth, 2013). Modelled T units were converted from energy unit (Wm^{-2}) to water depth unit (mm/day) for consistency by scaling the latent heat of vaporization to the growth chamber temperature.

The scaling coefficient α in Equation 1 accounts for the differences in optical absorbance properties between the leaf and the DRS. While Jones et al. (2018) set the value at 0.5, it is expected that the optical properties of the leaf will change according to both drought and nutrient status leading to a changes in emissivity. To account for these changes we developed a new vegetation index: the Combined Nitrogen and Drought Index (CNDI) which reflects changes in LWC and or N status as plants become increasingly stressed (Figures 7 and 8). Wavelengths used to calculate CNDI were obtained via PLSR and variable influence on projection (VIP) analyses of 6 different leaf traits and fluxes measured at Days 82 or 83 (Figure 6). At this stage in the experiment, wheat plants were either well-watered and fertilised, droughted and previously fertilised, well-watered and not fertilised or droughted and not previously fertilised. Using CNDI, we derived a dynamic scaling factor by integrating CNDI values into the sigmoid function set out beneath (Equation 4). A dynamic scaling factor (SF) was used to replace the α scaling factor (Equation 1) used by Jones et al. (2018).

$$SF = \left[x + \frac{1}{(1 + e^{-y\times(CNDI-z)})}\right]. \quad (4)$$

The coefficients: x, y and z of the sigmoid function are estimated using a nonlinear optimization; generalized reduced gradient (GRG) method. The optimum values of the coefficients of sigmoid function are determined by taking root-mean-square error (RMSE) as an

FIGURE 1 Leaf, plant and canopy-level impacts of wheat plants exposed to nutrient deficiency and or drought treatment. (a) Experimental overview of the drought and nutrient treatments. (b) RGB image of the four different treatments at Day 83. (c) Leaf stomatal conductance to water vapour values. (d) Thermal images of the four different treatments taken at Day 83, showing the hemispherical reference surface in the top right corner of each image. (e) Leaf temperature differences relative to the reference surface of four treatments. (f–i) Leaf level Normalized Difference Vegetation Index (NVDI), (g) leaf-level MERIS Terrestrial chlorophyll index (MTCI), (h) leaf area index (LAI) and (i) plant height measurements. Error bars equal ±1 SE. For simplicity, notations implying significant differences between treatments have not been applied to graphs. See Supporting Information S1: Figure 1 for statistical analysis. For (c, e–g), $n = 32$, for (h) 24 measurements per canopy were taken, and for (i), $n = 10$.

objective function during optimization. The sigmoid function in the model parameterization leads to a particularly lower modelled T for highly stressed plants, and also corrects for leaves that are a darker green than the DRS (indicative of very healthy leaves). This robust parameterization method corrects for both water limitation and/or nutrient/N deficiencies that might be impacting on the estimation of T. The updated formula for modelling T is as follows:

$$T_{CNDI} = \rho C_p SF g_{HR}(T_{dry} - T_c). \quad (5)$$

2.7 | Crop water stress estimation

To measure crop water stress, we calculated the crop water stress index (CWSI; Katimbo et al., 2022) by measuring leaf temperature to acquire T_c, T_{dry} and wet canopy temperature (T_{wet}) using thermal imaging and computed CWSI using the following equation:

$$CWSI = \frac{T_c - T_{dry}}{T_{wet} - T_{dry}}. \quad (6)$$

3 | RESULTS

The structural, physiological and optical response of wheat (*Triticum aestivum L*) plants to individual and combined nutrient and water stress are shown in Figure 1. During Days 35–60, the impacts of high N nutrient fertiliser addition are visible. From Days 60–83, the additional impacts of water stress are included to give four treatments: fertilised, watered (FW); fertilised, droughted (FD) unfertilised, watered (UW); and unfertilised, droughted (UD).

During Days 35–60, Figure 1 shows the impacts of N-fertiliser addition on water fluxes, leaf optical properties and plant structural characteristics. After 1 week (Day 42), plants not supplied with high N nutrient fertiliser had significantly reduced g_{sw} (Figure 1c, Supporting Information S1: Figure 1; t test, $p < 0.0001$), which corresponded to increased leaf temperature relative to the DRS (Supporting Information S1: Figure 1, t test, $p < 0.05$). Differences in both g_{sw} and leaf temperature continued to significantly differ between fertilised and unfertilised plants, with unfertilised plants showing a particularly marked reduction in g_{sw} (Figure 1c,e, Supporting Information S1: Figure 1). To assess leaf optical differences between treatments we calculated leaf normalized difference vegetation index (NDVI) and MERIS Terrestrial chlorophyll index (MTCI) from hyperspectral data. We chose these two indices for their known sensitivity to leaf area index (NDVI) and chlorophyll content (MTCI) (Huang et al., 2021; Viña et al., 2011). Both indices showed decreased values for unfertilised plants relative to fertilised plants by Day 42 (Figure 1f,g, Supporting Information S1: Figure 1; NDVI: t test, $p < 0.05$, MTCI: t test, $p < 0.0001$). For NDVI this trend was not observed at Day 60 (Supporting Information S1: Figure 1), but for MTCI there was an increasingly large difference between the values of fertilised and unfertilised plants. Lack of fertiliser also led to fewer leaves per unit area (Figure 1h) and smaller plants (Figure 1i), with significant differences for LAI and plant height detectable by Days 42 and 49, respectively (Supporting Information S1: Figure 1).

Imposition of drought at Day 60 resulted in a swift reduction in g_{sw} for FD plants (Figure 1c), with a significant difference detected comparatively to FW plants by Day 68 (Figure 1c, Supporting Information S1: Figure 1; t test, $p < 0.0001$). Assessment of leaf temperature differences at an equivalent stage (Day 69), showed that FW plants were significantly cooler than FD equivalent plants indicative of stomatal closure (Figure 1e, Supporting Information S1: Figure 1; $p < 0.0001$). Near the end of the drought (Day 82), FD plants had leaf g_{sw} values very close to 0 with markedly increased leaf temperatures (Day 83) (Figure 1c,e, Supporting Information S1: Figure 1). For leaf NDVI measurements, drought was only detectable in FD plants by Day 82 (t test, $p < 0.01$), whereas for MTCI, a drought signal was present by Day 76 (Figure 1f,g and Supporting Information S1: Figure 1; t test, $p < 0.01$). Removal of water led to lower LAI in FD plants by Day 68, and plant wilting and lack of growth resulted in FD plants being significantly shorter by Day 76 (Figure 1h,i, Supporting Information S1: Figure 1; t test, $p < 0.0001$). For UD plants that had not previously received high N nutrient fertiliser, a continually reducing g_{sw} (and increase in temperature) did not occur during drought (Figure 1c,e, Supporting Information S1: Figure 1). Only at Day 82 did UD plant g_{sw} show a significant reduction comparatively to UW plants (which had continued to receive water, Figure 1c,e, Supporting Information S1: Figure 1; $p < 0.01$) but this was not the case for UD plant leaf temperature, which remained similar to UW plants. For LAI and NDVI, UD values were also lower comparatively to UW plants, whereas for MTCI and plant height, values remained similar between unfertilised plants (Figure 1f–i, Supporting Information S1: Figure 1). Overall, FD plants were severely affected by the drought relative to FW plants, whereas for UD plants, only minor drought responses were detectable compared to UW control plants.

3.1 | The unequal contribution of leaf sides to wheat stomatal gas exchange

Previous work in wheat has shown that the adaxial leaf surface potentially contributes more to stomatal gas exchange than the abaxial surface (Wall et al., 2022). To ascertain whether this was also the case under different fertilisation regimes, we compared stomatal size (SS) (via stomatal length measurements), stomatal density (SD) and g_{sw} of both leaf surfaces (Figure 2). High N nutrient fertilisation resulted in an overall increase in SS and decrease in SD comparatively to unfertilised plants (two-way ANOVAs, SS: $p < 0.001$ and SD: $p < 0.05$; Figure 2a–d). The adaxial leaf surfaces of both fertilised and unfertilised plants had larger SS and higher SD than on abaxial surfaces (two-way ANOVA, SS: $p < 0.01$ and SD: $p < 0.001$; Figure 2a,b). When the g_{sw} of both sides were compared throughout the season it was apparent that the majority of gas exchange took place on the adaxial surfaces for both fertilised and unfertilised plants, with the abaxial values of either treatment rarely exceeding 0.1 mol m^{-2} s^{-1} (Figure 2e,f).

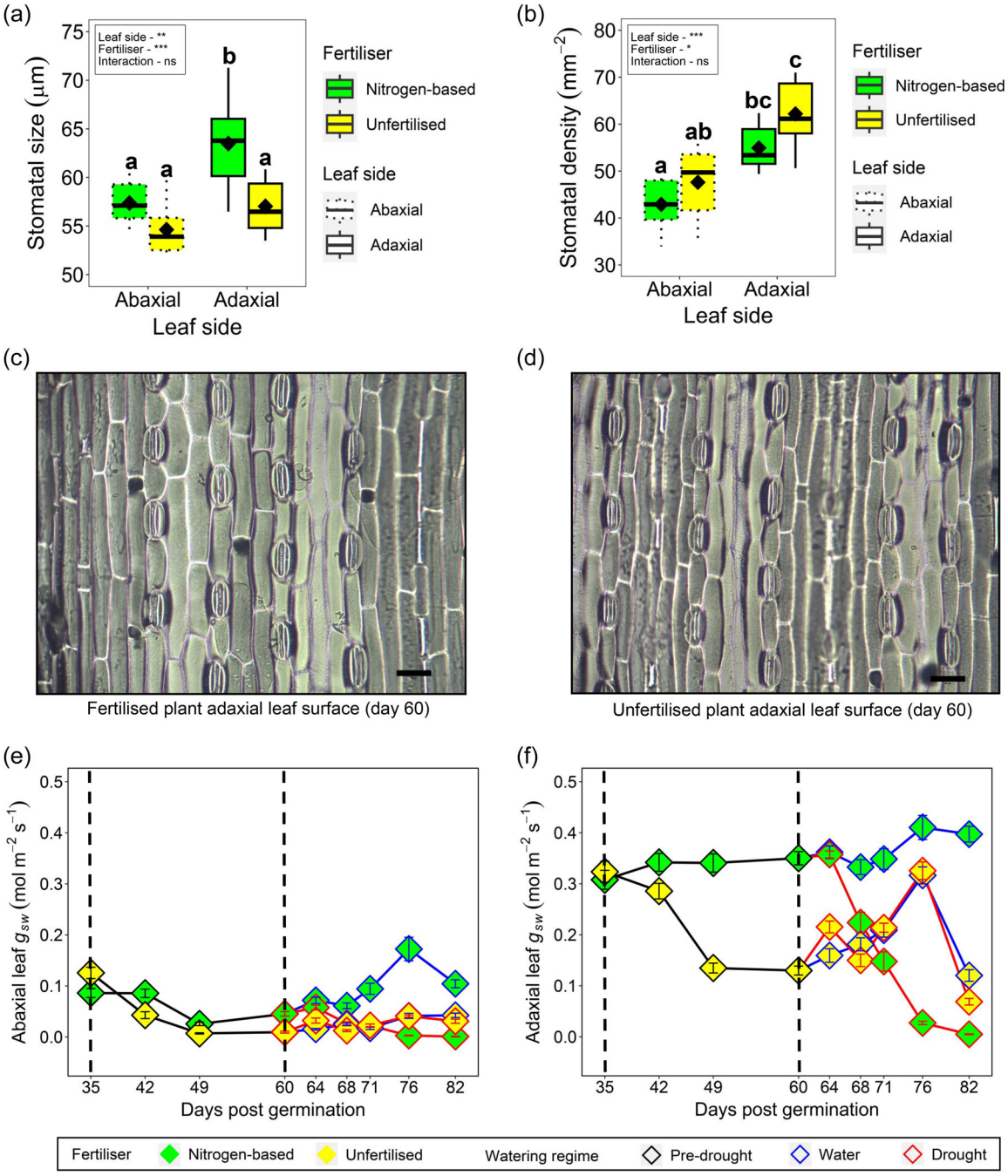

FIGURE 2 Anatomical and physiological assessment of both leaf surfaces of plants grown under different fertiliser regimes. (a) Stomatal size and (b) stomatal density on abaxial and adaxial leaves of fertilised and unfertilised plants. Representative images of (c) fertilised and (d) unfertilised adaxial leaf surfaces. Stomatal conductance measurements (e) abaxial and (f) adaxial leaf surfaces of fertilised and unfertilised plants across the experiment. For (a and b), two-way ANOVAs, post hoc Tukey tests were undertaken. Boxplot whiskers indicate variability at the upper and lower extremes and different letters on graphs indicate significant differences between means (p at least <0.05). Diamonds represent sample means. For (a and b), $n = 8$, for (e and d) $n = 32$. Scale bars in (c and d)=50 µm.

3.2 | Infrared gas analyser assessment of plant biochemical and physiological traits according to water and or nutrient stress

To further investigate how plant gaseous exchanges responded to differences in drought and/or nutrient deficiency, we used infrared gas analysers (IRGA) to measure photosynthesis (A), g_{sw}, intrinsic water-use efficiency (iWUE), the maximum carboxylation rate of rubisco (V_{cmax}) and the maximum rate of electron transport (J_{max}) (Figure 3).

As expected, plants grown with high N nutrient fertiliser had significantly higher rates of A, g_{sw}, V_{cmax} and J_{max} than unfertilised plants

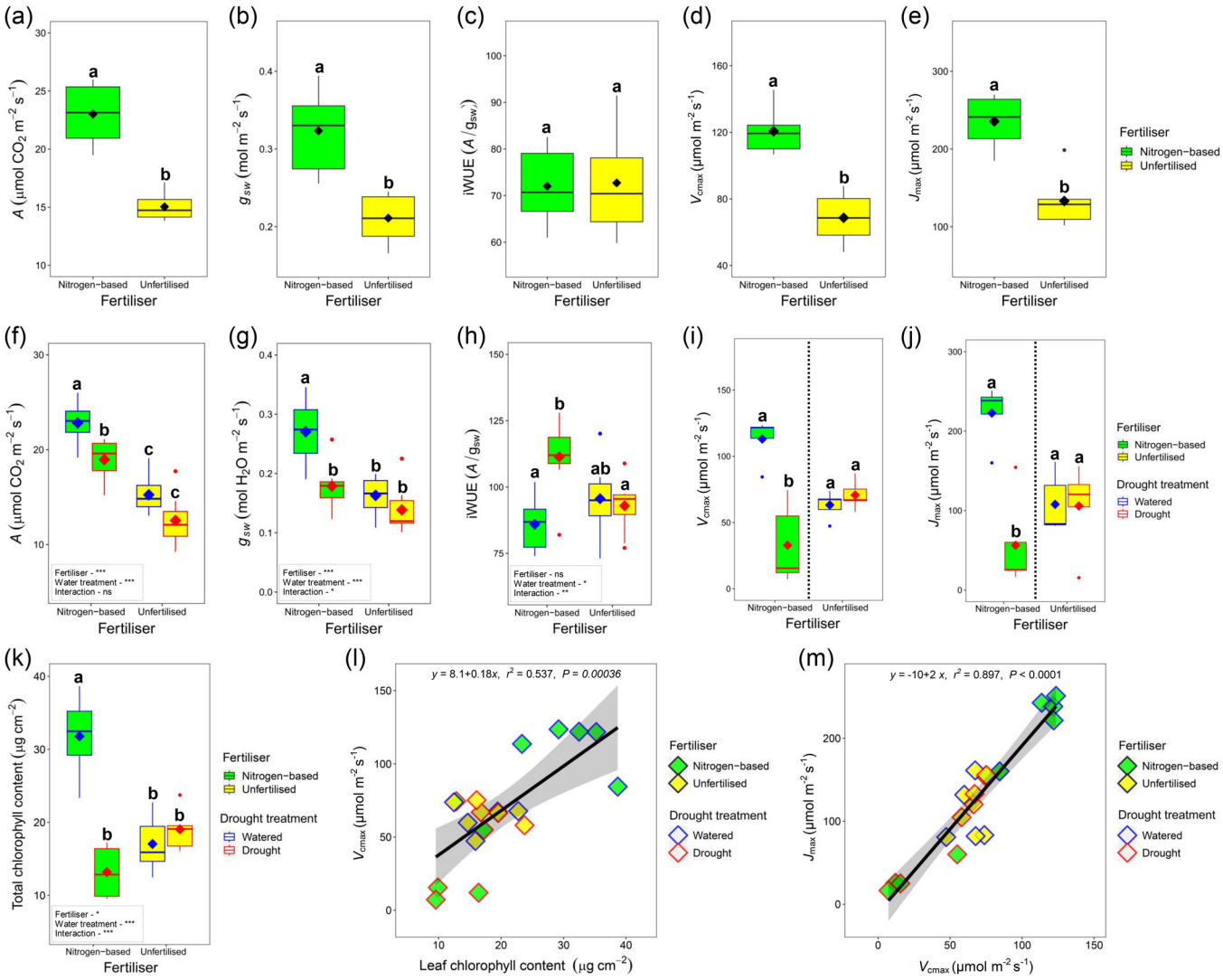

FIGURE 3 Leaf level gas exchange assessment showing adaptive changes in response to nutrient deficit and/or drought. (a–e) Initial gas exchange measurements conducted on fertilised or unfertilised measurements before drought assessing (a) photosynthesis (*A*), (b) stomatal conductance (g_{sw}), (c) intrinsic water-use efficiency (iWUE), (d) maximum carboxylation rate of rubisco (V_{cmax}) and (e) maximum electron transport rate (J_{max}). (f–h) Early drought gas exchange at Days 68–70 measuring (f) *A*, (g) g_{sw} and (h) iWUE. (i and j) V_{cmax} and J_{max} conducted on later stage drought at Days 76–77 and (k) leaf chlorophyll content at Days 76–77. (l and m) Regression analyses between (i) V_{cmax} and chlorophyll content and (m) V_{cmax} and J_{max}. Boxplot whiskers indicate variability at the upper and lower extremes and different letters on graphs indicate significant differences between means (p at least <0.05). Diamonds represent sample means. For (a–e), Students *t* tests were performed, for (f–k) one-way ANOVAs with post hoc Tukey HSD tests were undertaken. For (a–h), $n = 8$, for (i–m) $n = 5$.

(Figure 3a,b,d,e), but no significant differences were detected for iWUE (Figure 3c). To assess the impacts of nutrient deficiency combined with drought stress we measured plants at earlier (Day 9) and later stage (Day 16) of the imposed drought (Figure 3f–j). There was a significant reduction in all measured parameters for FD plants following drought treatment relative to FW plants (Figure 3f–j). Conversely, drought onset had no significant impact on UD plants relative to UW plants. For V_{cmax} and J_{max} measurements taken at drought Days 16–17, values of FD plants dropped markedly being significantly lower than FW plants (Figure 3i,j). The relationship between V_{cmax} and chlorophyll content, and V_{cmax} and J_{max} remained on the same slope, which indicates that the plants had not altered their N allocation strategy between photosynthetic N pools according to drought or N stress caused by lack of high N nutrient fertiliser (Figure 3k–m).

3.3 | Modelling stress-imposed trait acclimations using hyperspectral vegetation indices

To assess if optical remote sensing data could be used to detect the biochemical and physiological shifts in response to nutrient and/or water limitation, we first tested a subset of commonly used hyperspectral indices against plant biochemical and physiological traits measured at Days 16–17 of the imposed drought (Figure 4).

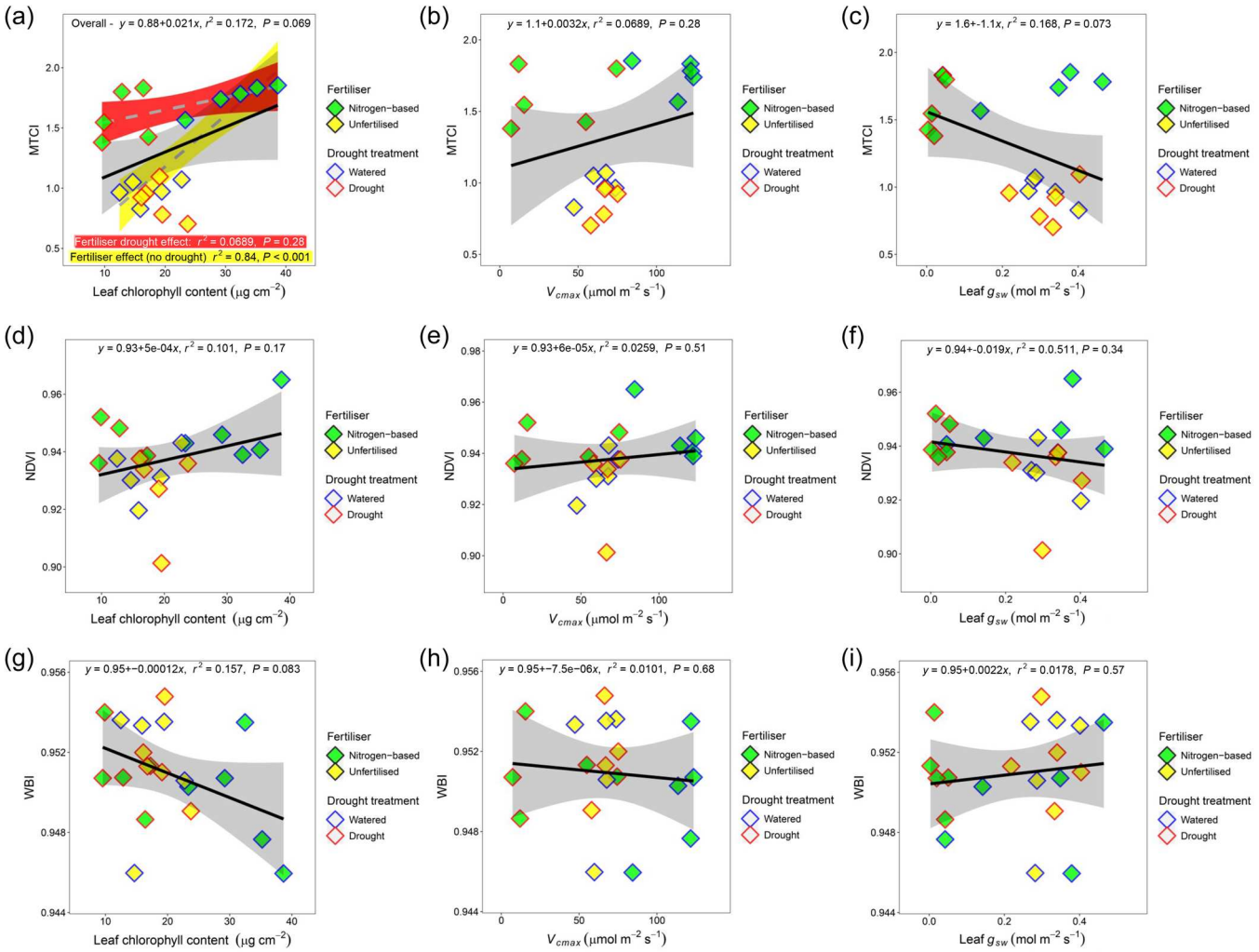

FIGURE 4 Assessment of potential relationships between leaf biochemical, physiological and water-related traits and leaf-level spectral vegetation indices on plants exposed to nutrient deficiency and/or drought. (a–c) Regression analyses of MERIS terrestrial chlorophyll index and (a) leaf chlorophyll content, (b) maximum rate of rubisco carboxylation (V_{cmax}) and (c) leaf stomatal conductance (g_{sw}) (d–f) Equivalent regressions comparing Normalized Difference Vegetation Index with (d) leaf chlorophyll content, (e) V_{cmax} and (f) leaf g_{sw}. (g–i) Water Balance Index regression analysis with (g) leaf chlorophyll content, (h) V_{cmax} and (i) leaf g_{sw}. No significant relationships between the three VIs and measured leaf traits were detectable. Measurements collected between Days 76–77. $n = 5$.

The results in Figure 4 demonstrate that vegetation indices (VIs) such as MTCI, NDVI and water balance index (WBI) do not typically represent good proxies for plants traits such as leaf chlorophyll content, V_{cmax} and g_{sw} under nutrient and drought stress. Differences caused solely by high N nutrient fertiliser application often had the potential to lead to significant relationships between VIs and biochemical traits (e.g., Figure 4a; MTCI vs. leaf chlorophyll, yellow regression line: $r^2 = 0.84$; $p < 0.001$), but such relationships broke down when both nutrient treatment and drought effects were considered simultaneously (Figure 4a; MTCI vs. leaf chlorophyll black regression line: $r^2 = 0.172$; $p = 0.069$). This was often due to FD plants not displaying a linear relationship with FW plants (e.g., Figure 4a; red regression line: $r^2 = 0.0689$; $p = 0.28$). Such failures of VIs to model plant traits under multiple abiotic stresses potentially limits the applicability of optical remote sensing for capturing deficiencies arising in heterogenous fields where water and nutrients (including N) might be simultaneously limited.

3.4 | Identifying unique spectra associated with multiple abiotic stresses via partial least squares regression analysis of optical hyperspectral data

The impacts of drought and/or nutrient deficiency at the end of the experiment (at Day 82/83) on selected leaf traits, including chlorophyll, N and LWC, δ13C, leaf temperature and adaxial leaf g_{sw} are displayed in Figure 5 (for latter two traits see also Figures 1e, 2f and Supporting Information S1: Figure 1).

FD plants had significantly less leaf chlorophyll, N and LWC than FW equivalents, whereas $\delta^{13}C$ values were significantly increased for

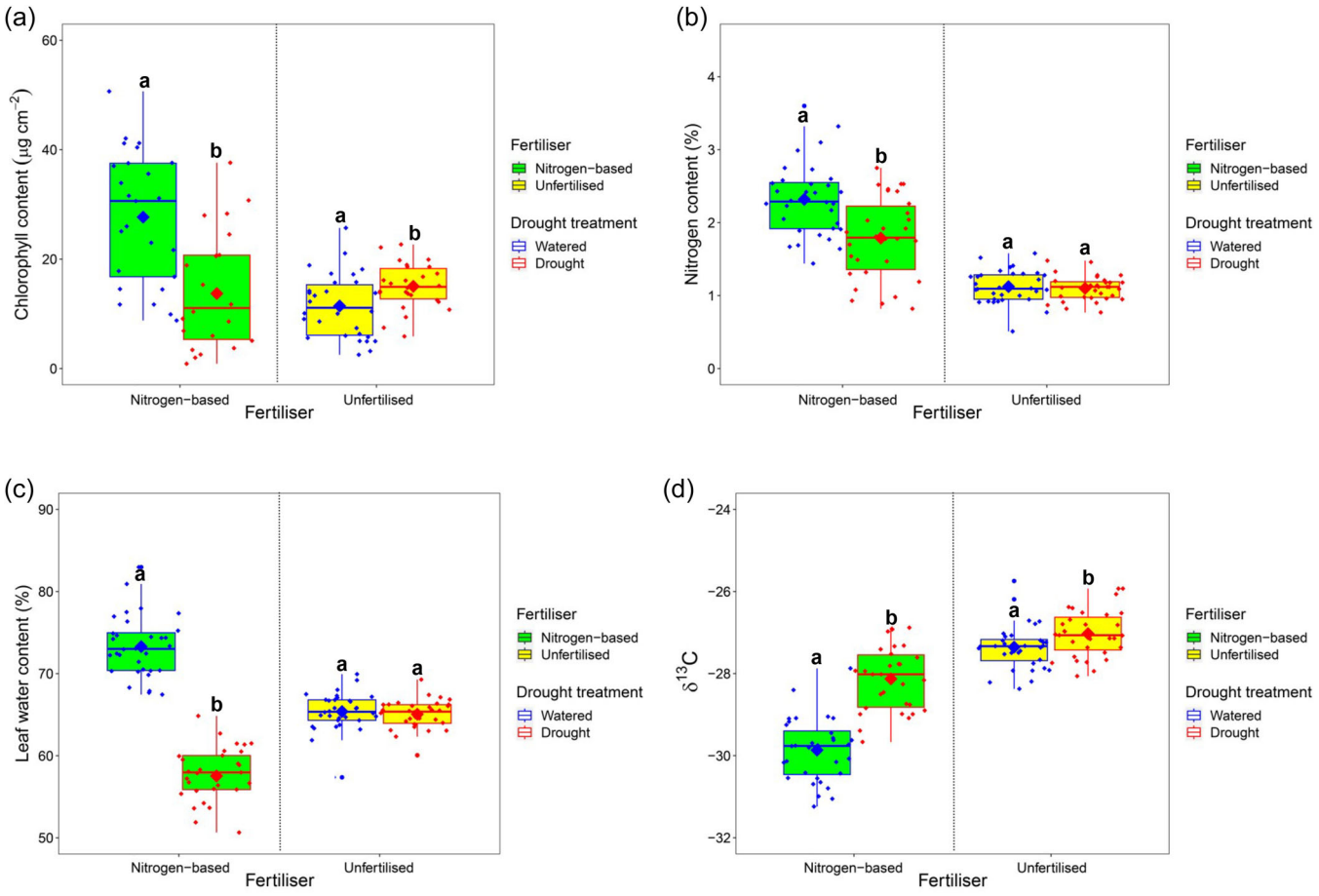

FIGURE 5 Leaf biochemical and water-related traits of plants exposed to nutrient deficiency and/or drought treatment at experiment Day 82. (a) Leaf chlorophyll, (b) nitrogen, (c) leaf water content and (d) δ13C. Boxplot whiskers indicate variability at the upper and lower extremes and different letters on graphs indicate significant differences between means (p at least <0.05). Due to unequal variances in all four traits measured, Student's t tests were performed to assess drought impact for a given nitrogen fertiliser treatment (separately analysed samples divided by dashed lines). $n = 32$.

FD, indicative of better water-use efficiency during the drought comparatively to FW plants (Figure 5). For UD plants we detected an increases in both chlorophyll content and $\delta^{13}C$ values relative to UW controls, whereas N content and LWC remained unchanged. The strength of PLSR modelled results for each trait (Figure 6a,c,e,g,i), along with wavelengths that show the strongest relationships with the respective traits are highlighted via variable influence on projection (VIP) plots (Figure 6b,d,f,h,j).

Results of traits measured at Day 82/83 showed chlorophyll content to have the weakest relationship with reflectance spectra (Figure 6a; $R^2 = 0.44$, RMSEP 7.35, %RMSEP = 17.84), whereas N content (Figure 6b; $R^2 = 0.6$, RMSEP 0.36, %RMSEP = 16.28), g_{sw} (Figure 6c; $R^2 = 0.65$, RMSEP 0.1, %RMSEP = 18), leaf temperature difference (Figure 6d; $R^2 = 0.59$, RMSEP 0.6, %RMSEP = 14.59) and $\delta^{13}C$ (Figure 6e; $R^2 = 0.65$, RMSEP 0.77, %RMSEP = 14.54) had stronger relationships. Overall, measured LWC had the strongest relationship with hyperspectral reflectance (Figure 6f; $R^2 = 0.84$, RMSEP 2.8, %RMSEP = 8.36). VIP analysis of all six traits revealed distinct absorption features most related to the measured biochemical traits and water-related fluxes (Figure 6g–l). Wavelengths at R_{706}, R_{1402}, R_{1451} and R_{1878} were identified as key spectra for describing differences in N and/or drought treatment, with all four peaks being clearly detectable on leaf g_{sw}, temperature difference and LWC VIP graphs (see Figure 6l for peak markings). For leaf chlorophyll content, N content and $\delta^{13}C$ VIPs, R_{706} values were larger, whereas the other three identified peaks were less pronounced or close to undetectable. Previous research has shown that R_{706} is in the red-edge region known to be particularly sensitive to leaf chlorophyll content and thus useful for measuring biochemical traits (Curran et al., 1990). To assess whether R_{706}, R_{1402}, R_{1451} and R_{1878} might also be important for modelling drought over time, we also employed PLSR to assess individual treatments over the duration of the drought. We found in FD plants specifically, that g_{sw} and leaf temperature VIP plots identified the same four wavelengths as being important (Supporting Information S1: Figures 2 and 3).

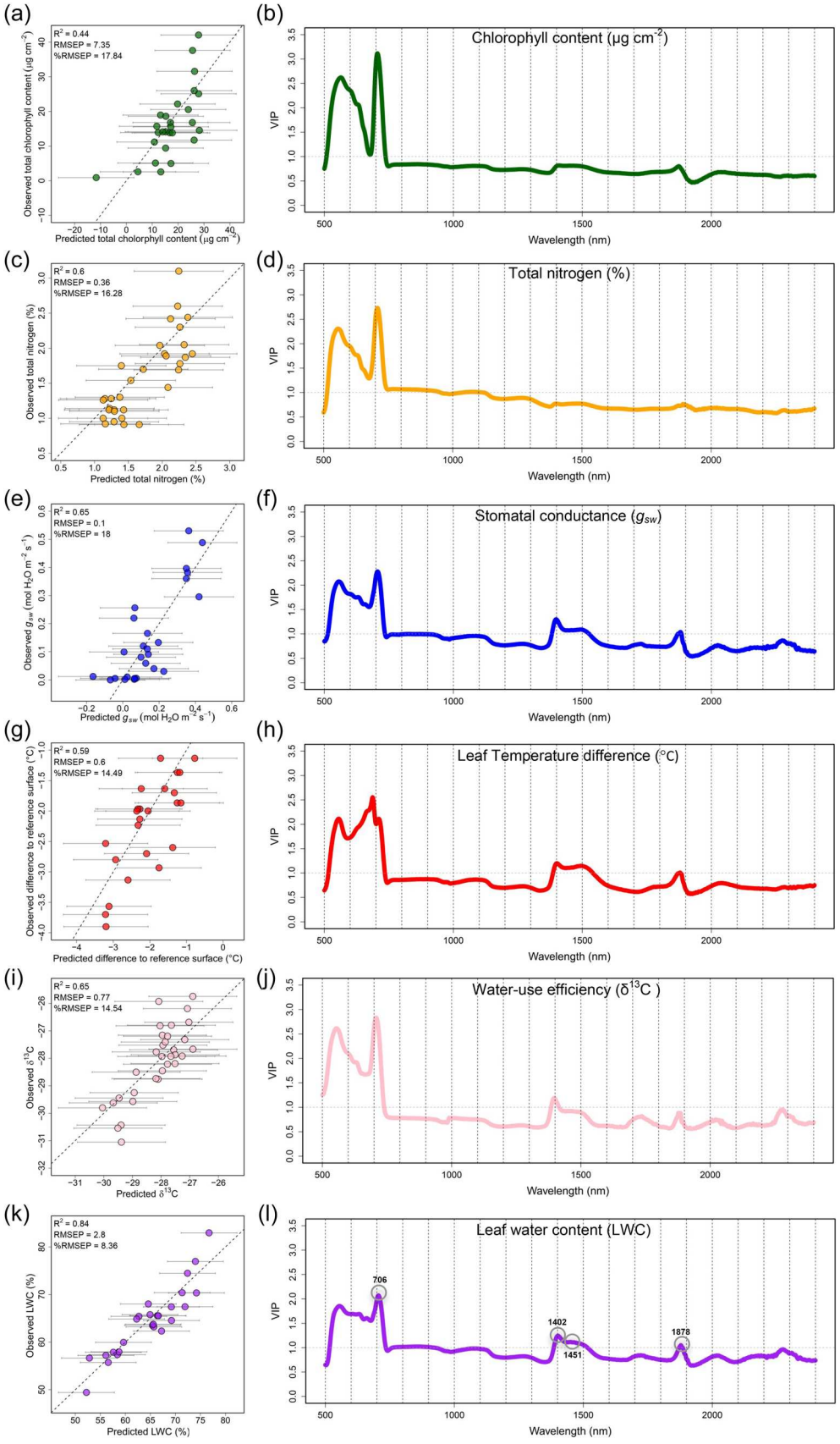

FIGURE 6 (See caption on next page).

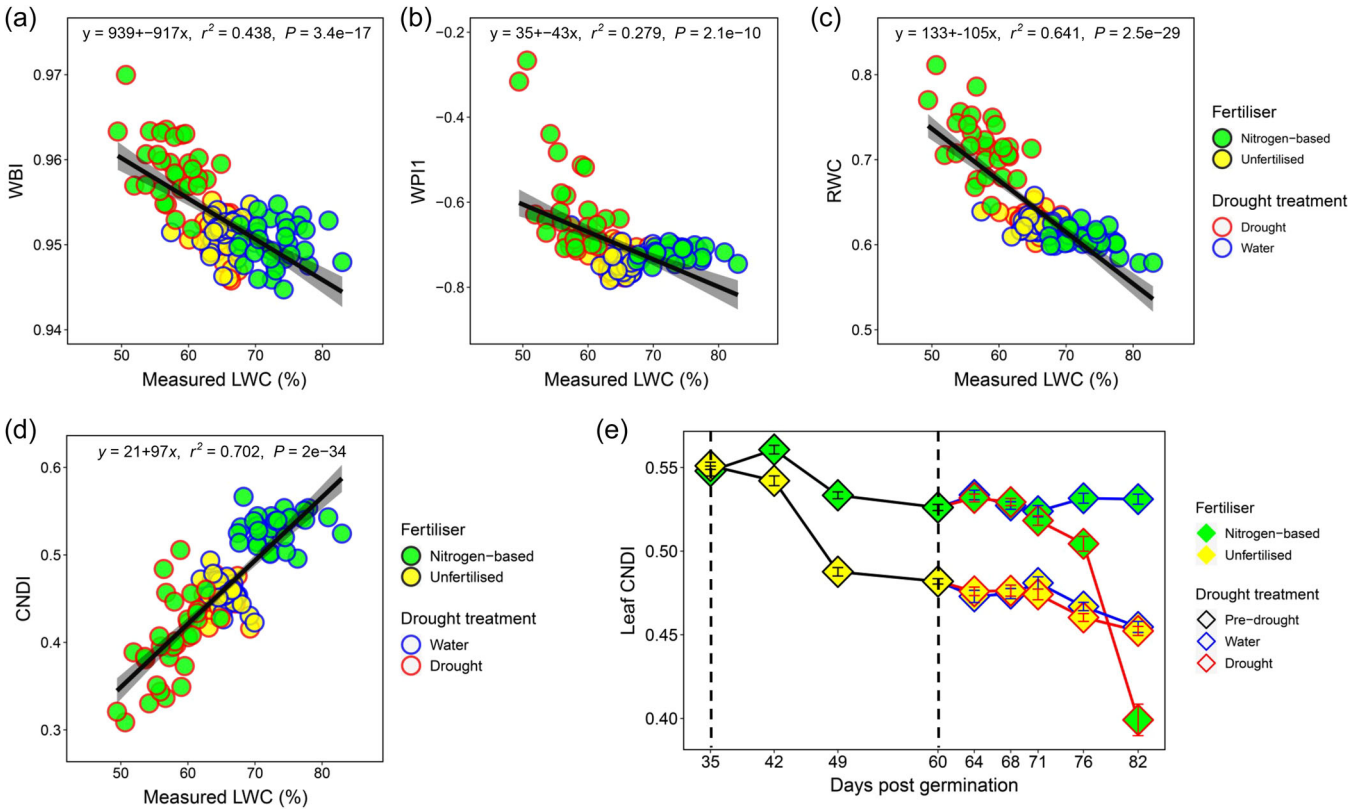

FIGURE 7 The Combined Nitrogen and Drought Index (CNDI) models changes in leaf water content (LWC) caused by nitrogen and/or drought stress. (a–d) Regression analyses of measured leaf LWC with the following vegetation indices: (a) Water Band index (WBI), (b) Water Potential Index 1 (WPI1), (c) Relative water content (RWC) (d) CNDI. (e) CNDI values calculated via hyperspectral data over the duration of the experiment. $n = 64$ before drought and 32 once drought has begun. Error bars equal ±1 SE.

3.5 | A new multi-stress vegetation index for identifying drought and or nitrogen stress

The difficulty in using VIs to model leaf traits under different types of abiotic stress are demonstrated in results from this study (Figures 4 and 6), and in previous work (Croft et al., 2014; Gerhards et al., 2016). To address this issue, we leverage biochemical information from different spectral regions identified in Figure 6 to develop a new VI that is sensitive to LWC under different nutrient and or drought stress. The CNDI (Equation 7) is calculated from the four identified wavelengths in Figure 6 along with a normalising wavelength (R_{1353}), which is insensitive to water and N content:

$$\text{CNDI} = (R_{1353}/(R_{706} + R_{1402} + R_{1451} + R_{1878})). \quad (7)$$

The relationship between CNDI and measured LWC shown in Figure 7 confirms that CNDI more accurately describes measured LWC ($r^2 = 0.702$; $p < 0.0001$) than a variety of other previously published VIs that look at leaf water properties (Mertens et al., 2021; Figure 7a–d). CNDI also accurately predicted LWC changes as stomata reached closure during drought (at Day 76; $r^2 = 0.427$; $p < 0.01$), but this was not the case for the other VIs we surveyed (Supporting Information S1: Figure 4). When viewed over the duration of the experiment, CNDI initially detects significant differences between high N nutrient fertiliser treatments by Day 42 of the experiment (Students t test, $p < 0.0001$), and this difference gradually increases over time until for FD plants, the drought effect causes CNDI to fall rapidly as leaves dry out (Figure 7e).

Our CNDI data shows that healthy green wheat leaves have a CNDI value of above 0.5 (0.52–0.56 in our growth rooms) whereas during stress, CNDI gradually falls, which by the end of the experiment resulted in CNDI mean values of 0.45 for nutrient deficient plants and 0.38 for FD plants. To understand whether CNDI has the potential to be used more broadly to understand plant stress,

FIGURE 6 Partial least squares regression (PLSR) and variable influence on projection (VIP) analysis identify hyperspectral signatures involved with drought and/or nutrient deficiency. (a–l) PLSR and VIP analysis of (a and b) leaf chlorophyll content, (c and d) % nitrogen content, (e and f) stomatal conductance to water vapour (g_{sw}), (g and h) leaf temperature difference relative to the dry reference surface, (i and j) δ13C and (k and l) leaf water content. Wavelengths with a VIP of above 1 were highlighted as being particularly important for downstream phenotyping: 706, 1402, 1451 and 1878 nm. $n = 128$.

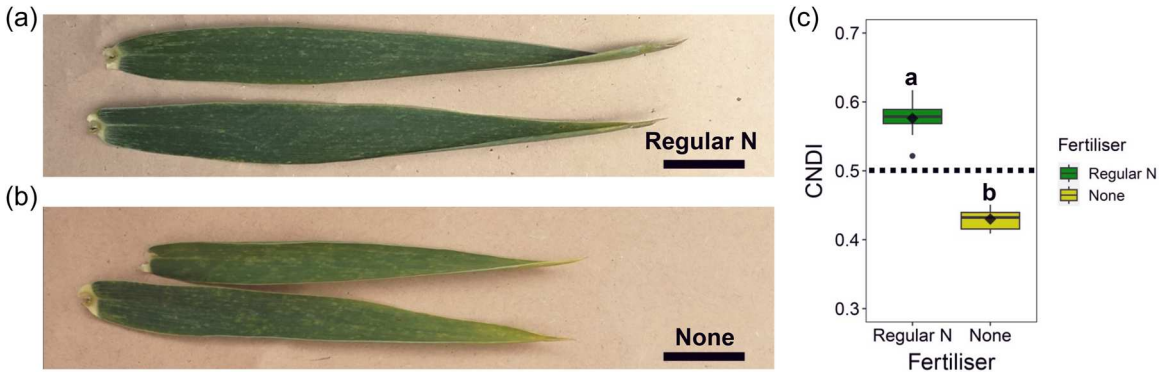

FIGURE 8 Combined Nitrogen and Drought Index (CNDI) assessment of field-grown wheat grown under differing nitrogen fertiliser application. Representative leaf images of (a) regular fertiliser application (regular N) or (b) no fertiliser application (none). (c) CNDI values of wheat grown with regular N or no fertiliser application. The dashed line denotes a CNDI of 0.5. Boxplot whiskers indicate variability at the upper and lower extremes and different letters on graphs indicate significant differences between means (p at least <0.0001, Wilcoxon rank sum exact test). $n = 15$. Scale bars in (a and b)=2 cm.

we calculated CNDI from several additional hyperspectral data sets, starting first with field-grown wheat which differed in N fertiliser application (Figure 8). We found that flag leaves of N fertilised plants had a mean CNDI of 0.58 whereas unfertilised equivalent plants had a significantly lower CNDI mean of 0.43 (Students t test, $p < 0.0001$) (Figure 8a–c). These values are in accordance with what we would expect based on the data generated in our growth chamber experiments.

To investigate whether CNDI might also be applicable for use with assessing stress in other crops, we assessed data relating to the drought responsiveness of different glasshouse-grown crops via hyperspectral data made freely available by Burnett et al. (2021b) (Supporting Information S1: Figure 5). Both cayenne pepper (*Capsicum annuum* L) and sorghum (*Sorghum bicolor* L) had higher MTCI values (2–4) than growth chamber-grown wheat MTCI (1.5–2, see Figure 1g). Based on the separation of RWC values, it seems that the overall drought stress experienced by cayenne pepper (which was droughted for longer) may have been greater than that of sorghum. Despite this, CNDI means both dropped below 0.5 by the end of the respective drought experiments (0.381 for cayenne pepper and 0.496 for sorghum) (Supporting Information S1: Figure 5). In both cases, values appeared to have not finished falling, but this was where the respective experiments were concluded. Fertilised nondroughted plants typically had CNDI values above 0.5, with cayenne pepper displaying values of 0.669–0.821 and sorghum having values of 0.595–0.689. These higher CNDI values appeared to be linked to higher MTCI values, meaning that both sets of glasshouse crops probably had dark green leaves when fertilised.

3.6 | Modelling leaf transpiration under multiple abiotic stresses

As we have shown, it is possible to employ hyperspectral remote sensing methods to detect changes in LWC when plants experience nutrient and/or water stress (Figures 6 and 7). However, optical reflectance values fail to capture dynamic fluxes associated with early stomatal closure during drought (as observed via porometry and thermal imaging at Days 68 and 69). Conversely, porometry and thermal imaging cannot differentiate between a partially droughted leaf and a nutrient deficient leaf when leaves are operating at similar level of water flux, which affects crop management decision making. Further, within thermal-based approaches, it is assumed that biochemical and structural properties of leaves are the same, but this research has shown that this might not always be the case (Figures 1–7). Combining hyperspectral and thermal imaging offers an opportunity to improve modelled water fluxes by integrating leaf reflectance parameters into current T models. This will in some ways counterbalance the erroneous temperature readings associated with lighter colours being cooler (Figure 9a) and thus assumed to have higher g_{sw}.

By building on the thermal-based model formulated by Jones et al. (2018) (Equation 1), we apply sigma factor transformed CNDI to replace the fixed α scaling factor, thus accounting for temporal and dynamic differences in leaf reflectance and emissivity (relative to the DRS) caused by the imposition of nutrient fertiliser N stress and/or drought stress (Figure 9b,c; Equations 4 and 5). We present in-situ modelled adaxial g_{sw} for all four treatments alongside average adaxial leaf T values modelled either via the original Jones model (T_{Org}) or the new T_{CNDI} model (Figure 9d–h). Overall the results show an improvement in modelled transpiration for the T_{CNDI} model across nutrient deficiency and/or drought conditions, with relationships against measured porometry-based (in-situ T) estimates of $r^2 = 0.46$ for T_{Org} ($p < 0.001$) and $r^2 = 0.61$ for T_{CNDI} ($p < 0.001$) (Figure 9g,h). To further assess the accuracy of T_{CNDI} for predicting measured in-situ T, we performed Repeated K-fold Cross Validation (Witten & James, 2013) and confirmed T_{CNDI} to be a good indicator of in-situ T when modelling water fluxes during nutrient deficiency and or drought ($k = 5$, repeats = 3, $r^2 = 0.641$, RMSE = 0.476, MAE = 0.372).

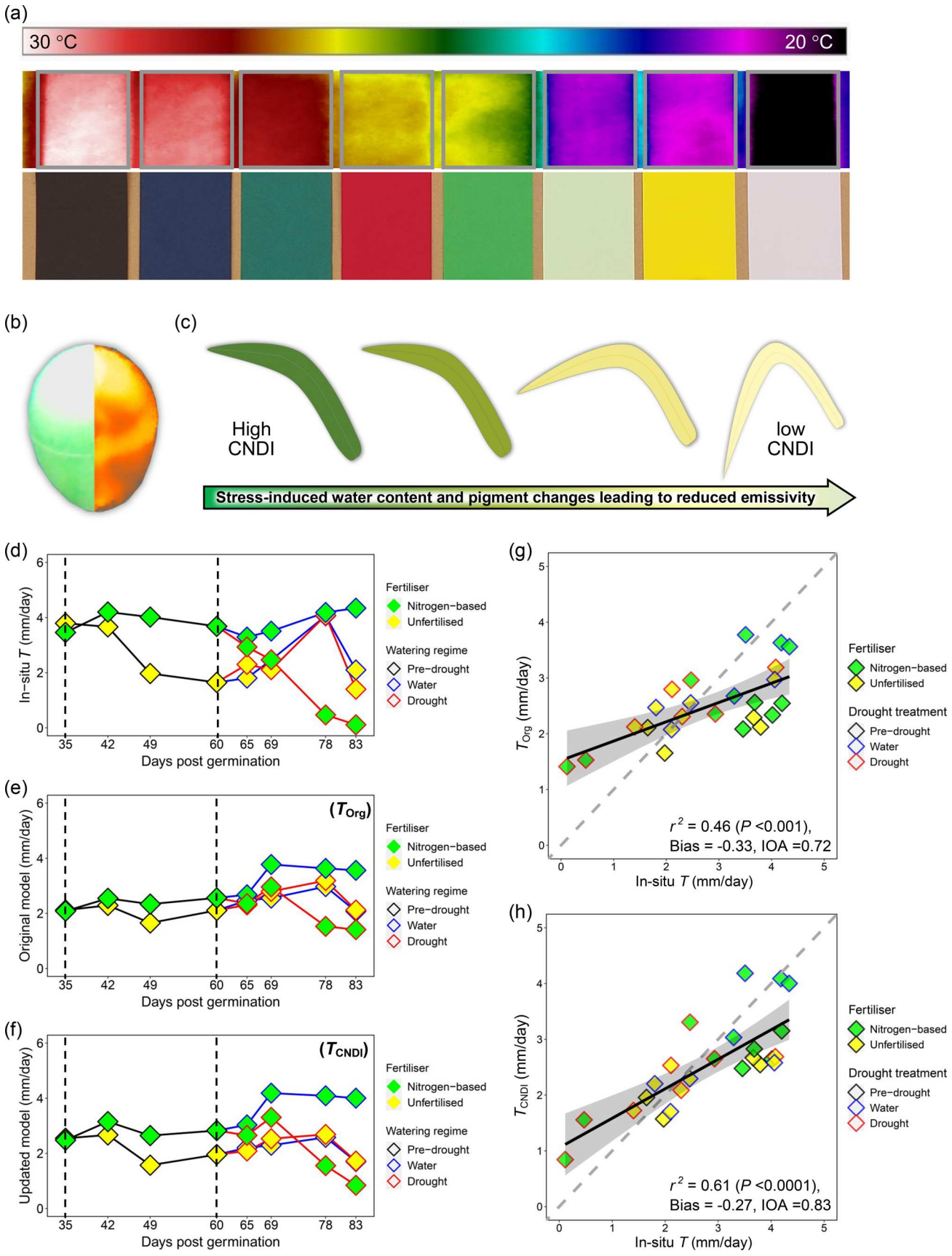

FIGURE 9 (See caption on next page).

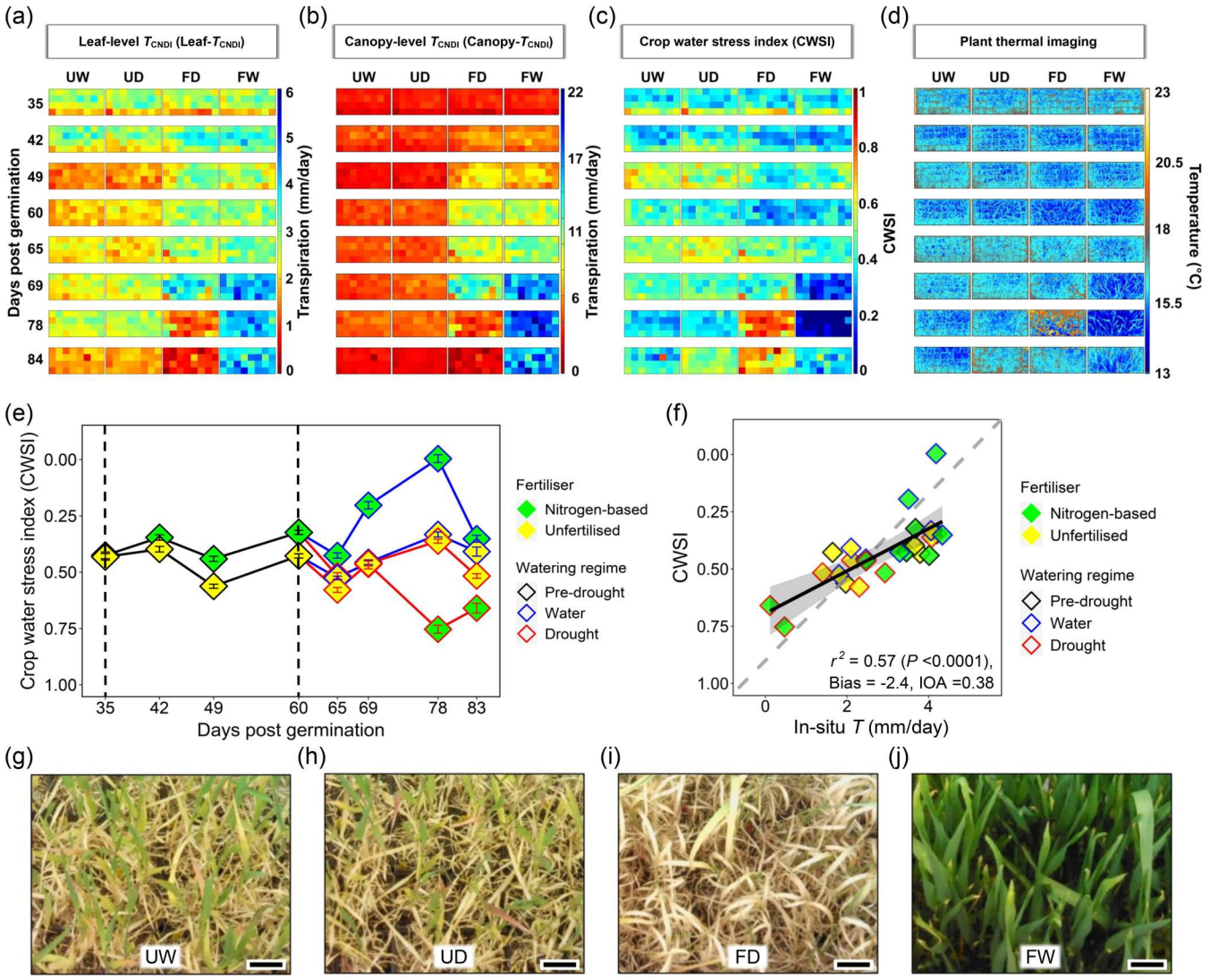

FIGURE 10 Spatio-temporal variations in water fluxes and water stress caused by nutrient deficiency and/or drought. (a–c) Heatmaps of (a) CNDI modelled leaf-level transpiration (Leaf-T_{CNDI}), (b) canopy-level transpiration (Canopy-T_{CNDI}) and (c) crop water stress index (CWSI). (d) Thermal images. (e) Crop water stress index over time (CWSI) and (f) regression analysis between CWSI and in-situ T based on stomatal conductance measurements. (g–j) RGB images at the end of the combined stress experiment of (g) UW = unfertilised, water treatment, (h) UD = unfertilised, drought treatment (i) FD = fertilised plants followed by drought and (j) FW = continual fertilised plants. Error bars equal ±1 SE. Scale bars = 5 cm.

3.7 | Spatio-temporal variations in leaf and canopy T and water stress

To ascertain how T_{CNDI} measurements and water stress measurements overlap both spatially and temporally, we present modelled T_{CNDI} at the leaf-level (Leaf-T_{CNDI}) and canopy-level (Canopy-T_{CNDI}) alongside an empirical, temperature index-based approach for measuring water stress at the leaf level: the crop water stress index (CWSI; Figure 10). Canopy-T_{CNDI} values were calculated using a 'big-leaf approach' for simplicity, where Leaf-T_{CNDI} values were multiplied by its proportionate fraction of LAI measurements.

FIGURE 9 Integrating transformed hyperspectral CNDI values boosts the accuracy of modelled leaf transpiration (T) modelling during nitrogen and/or drought stress. (a) RGB and thermal images highlighting differences in emissivity caused by differences in colour. (b) RGB and thermal image of the hemispherical dry reference surface (DRS) used to calculate leaf T_{dry}. (c) Schematic overview of nitrogen and/or drought stress impacts on leaf visible reflectance. (d) In-situ T based on stomatal conductance measurements collected over the duration of the experiment. (e) Original T modelled (T_{Org}) from Jones et al. (2018). (f) Updated T_{CNDI} model (g and h) Regression analyses between in-situ T measurements and (g) T_{Org} and (h) T_{CNDI}.

Assessment of both leaf and canopy T_{CNDI} models (Figure 10a,b) reveals the effects of N-based fertiliser application on total canopy *T*. For both Leaf-T_{CNDI} and Canopy-T_{CNDI}, high N nutrient fertiliser treatment increased water fluxes by Day 42 (compare FD and FW with UW and UD), leading to higher *T* levels. However, as canopies developed over time, the cumulative effect of fertiliser application is much more apparent in the Canopy-T_{CNDI} model, which accounts for the reduced number of leaves at the beginning of measurements. Comparisons between Leaf-T_{CNDI} and Canopy-T_{CNDI} responses and the thermally derived CWSI and raw thermal data responses reveal some similarities in detectable water flux versus water stress patterns, but as the drought became increasingly severe, this did not continue to be the case (Figure 10a–e). By Day 83, CWSI (and raw thermal images) no longer identified increasing water stress despite the sustained drought, instead water stress appeared reduced as plants appeared cooler on Day 83 than Day 78. For both Leaf-T_{CNDI} and Canopy-T_{CNDI}, *T* values continued to decrease indicating that water was becoming increasingly exhausted as plants dried out. Assessment of thermal and RGB images reveal that FD leaf angle and reflective properties, as well as canopy and structural changes caused by wilting, may well have been contributing to the discrepancies observed between CWSI and Leaf-T_{CNDI} and Canopy-T_{CNDI} measurements at Days 77 and 83 (Figure 10d,f). Compared to Leaf-T_{CNDI} (r^2 = 0.61) and T_{Org} (r^2 = 0.46) relationships with in-situ *T* (based on g_{sw} porometry data), the relationship between CWSI and in-situ *T* produced an r^2 of 0.57 (Figure 10f).

4 | DISCUSSION

4.1 | Plant gas exchange responses to nitrogen and/or water stress

In future climates where water and/or N will be increasingly limited, innovative approaches will be required that boost crop yields that at the same time minimises resource expenditure. Heterogeneity within fields will require robust mathematical modelling to optimise the spatial and temporal growth of our crops, and remote sensing technologies will be critical for providing accurate input data (Li et al., 2020; Plett et al., 2020; Sarić et al., 2022). Here, we have integrated a variety of different phenotyping technologies in unison to increase the accuracy of how plant water fluxes are modelled when two abiotic stresses are occurring concurrently. We observed sizeable differences in gas exchange between fertilised and unfertilised plants before drought (Figures 1–3), with adaxial leaf surfaces contributing to the majority of leaf g_{sw}. While our leaf surface analysis results broadly follow those of Wall et al. (2022), our porometry measurements highlight that under steady-state chamber conditions, that the abaxial leaf surface only had a small contribution to overall gaseous exchange. Why such partitioning of gas exchange occurs in wheat is intriguing, and further studies are required to elucidate the underpinning molecular and physiological mechanisms that regulate such processes.

The gas exchange differences we observed between fertilised and unfertilised plants seems to be inherently linked with differences in investment of N in light-harvesting pigments and RuBisCO biosynthesis (Kubar et al., 2022; Ookawa et al., 2004). Nutrient-limited N starvation reduced both *A* and g_{sw} under well-watered conditions comparatively to fertilised plants in our experiments, but this did not impact on iWUE that remained equal to fertilised plants. Similar *A*, g_{sw} and iWUE responses have previously been detected in poplar (Liu & Dickmann, 1996), but such responses are not always the same. Guehl et al. (1995) found in oak that all three gas-exchange parameters reduced, whereas in pine, g_{sw} actually increased whereas *A* and iWUE decreased. As others have detected before us (Seibt et al., 2008), we found that δ13C values do not necessarily follow the same pattern as iWUE measurements when N was limited, although during drought, FD plants did have increased δ13C and iWUE relative to FW plants as stomata were closing. Unfertilised plants had the highest values of δ13C, which is surprising given previous studies have shown that δ13C is typically linked with a higher N content (Cao et al., 2019; Verlinden et al., 2015). These data together highlight the complex nature of understanding plant water-use at the leaf level when multiple abiotic stresses are concurrently occurring.

Chlorophyll content has been shown to be a strong proxy for V_{cmax} owing in large part to the optimum investment of N across photosynthetic components (Croft et al., 2017; Wang et al., 2018), and this is supported here even under differing drought and nutrient treatments where N was limited. In our study, V_{cmax} measurements on FD plants were undertaken when stomata were nearly closed, which most probably led to reduced T restricting the flow of N to leaves (as evidenced by reduced N at Day 83), as chlorophyll was breaking down as water stress was increasing (Figure 5). We questioned whether commonly used hyperspectral indices such as MTCI, NDVI and WBI, which are routinely used in remote sensing approaches, could serve as good proxies for chlorophyll content and V_{cmax} during a dynamic drought scenario, but found no discernible relationships between any of the VIs and water stress. This result supports previous work also showing that VIs do not always serve as good markers for plant photosynthetic performance when water stress is introduced (Liu et al., 2018; Shiratsuchi et al., 2011). This latter finding highlights why caution must be taken when using VIs on a global level to interpret productivity when little information is known about the prevailing plant water status.

4.2 | Detecting multiple stresses simultaneously using remote sensing technology

In this study, we first addressed which phenotyping technologies were best at detecting the onset of early plant stress. Our results showed it was possible to detect differences in LAI, porometry, thermal imaging and hyperspectrally derived MTCI and NDVI from 1 week (42 dpg) after fertilisation had first been applied (Figure 1). Following drought imposition at Day 60 we did not detect such a uniform response between different phenotyping technologies, with

porometry and thermal imaging at Days 68–69 (and LAI at Day 68) being much quicker to identify drought stress than MTCI and NDVI (at Days 76 and 82 respectively). This finding is similar to those of Gerhards et al. (2016) who also found porometry and thermal measurements to be good markers of early water stress detection whereas optical imaging stress detection typically took longer. Recent research in maize has showed that hyperspectral stress detection can be complicated further due to overlapping reflectance signals of multiple stressors (in this case drought and western corn root worm; WRC) (Peron-Danaher et al., 2023). While the authors could detect WRC under well-watered conditions, this was not the case when drought was simultaneously applied, which highlighted the limitations of using hyperspectral imaging to study multiple stressors. We also found hyperspectral reflectance signal overlapped during combined drought and nutrient stress (particularly Days 76 and 82), which re-affirmed the limitations found by Peron-Danaher et al. (2023).

Using the full hyperspectral range of wavelengths within PLSR and VIP analysis of measured LWC (and five other trait and fluxes), we identified wavelengths at 706, 1402, 1451 and 1878 nm as being important for capturing phenotypic variations arising from drought and differences in leaf N and water content at Day 82/83 (Figures 5 and 6). Sun et al. (2022) also highlighted that changes in reflectance at 706 nm (and 688 nm) can identify N status under different watering regimes, due to the sensitivity of the red-edge region to chlorophyll and N content (Curran et al., 1990; Li et al., 2014). Two of the three VIP highpoints detected in the short-wave infrared (SWIR): 1402 and 1450 nm span regions often associated with differences in LWC and are regularly associated with drought (Carter, 1993; Gausman & Allen, 1973; Mertens et al., 2021; Seelig et al., 2008). The same is true of 1878 nm which is also often linked to equivalent water thickness, otherwise referred to as area-weighed moisture content (Cao et al., 2015). By combining reflectance from these sensitive wavelengths in the CNDI formula, it is possible to capture changes in leaf reflective properties associated with N and or drought stress to improve modelled plant water-use under both abiotic stresses (Figures 7–10). We have provided evidence that CNDI values could be applicable across different wheat growth environments and between different crop types (Figure 8, Supporting Information S1: Figure 5), but this is only a small sampling of single stress data sets, and so further research is still required to validate whether T_{CNDI} can be applied broadly across different environmental and crop scenarios where both drought and N deficiency are occurring simultaneously. It should be re-emphasised here that because g_{sw} typically decreases before LWC (and other biochemical changes associated with drought) (Bhusal et al., 2020; Du et al., 2012), that flux-based technologies such as thermal imaging are still very much key for capturing the earliest signs of plant water stress.

Currently most leaf spectroradiometers cover either the visible near infrared (VNIR; 400–1000 nm) or the SWIR (1000–2500 nm), and those that cover the full spectrum (400–2500 nm) are typically quite expensive (Liu et al., 2020; Sarić et al., 2022). For unoccupied aerial vehicles (UAVs) with hyperspectral cameras, including drones, this is especially the case, with technology that covers the full spectrum still under development (Oliveira et al., 2024; Saari et al., 2017). Both of these limitations (excessive cost and limited wavelength coverage) represent technological bottlenecks that are currently preventing indices such as CNDI from being employed over large scales. To obtain values of T from synergised optical and thermal data such as with T_{CNDI}, there is a need for remote sensing technology prices to fall and at the same time the speed of UAV innovations needs to accelerate. One shorter-term option for employing optical and thermal technologies together in the present would be to minimum–maximum normalise MTCI values and then use a sigma function to compute the most appropriate alpha scaling factor for thermal modelling. The downside to this approach would be that water band information from the SWIR would not be available and thus such an approach may well be less accurate, particularly when drought occurs.

4.3 | Balancing fertiliser application with water availability to maximise productivity

Despite receiving fertiliser, by Day 82 FD plants had the lowest chlorophyll and g_{sw} values of all the plants, with Leaf-T_{CNDI} and Canopy-T_{CNDI} values close to 0 and leaves that had markedly reduced LWC. This indicates that fertilised FD plants with higher LAI and T rates are much more susceptible to drought and closed stomata far more rapidly than UD plants (Figures 1, 5, and 10). These findings highlight the potential risk fertilisation application can have in drought-prone locations. Termed 'haying off', larger crop canopies have been shown to be more prone to prematurely drying out before forming grain, caused in large part due to the increased evaporative demand of a larger vegetative biomass (Van Herwaarden et al., 1998). On the other hand, it has also been shown that wheat crops that do not receive enough fertiliser early in the season fail to produce maximal yields when water is plentiful later in the season (Plett et al., 2020; Van Herwaarden et al., 1998). Insufficient N application can also reduce grain protein content due to excessive nutrient leaching when water is plentiful, further complicating the balance between applying the correct amount of fertiliser and managing plant water-use. Clearly, to optimise fertiliser use and maximise grain yields, plant water-use and water availability, along with N availability, must be considered both before and throughout the growing season.

5 | CONCLUSION

Temperature-based energy balance T models are capable of dynamically modelling water fluxes due to the evaporative cooling effects of stomatal-regulated water release on leaf temperature. To overcome the difficulty in obtaining net radiation, a DRS is used to normalise the canopy surface temperatures. We have shown that a key limitation of this method is that the reflectance properties of the leaves and canopies may change over time and depart from those of

the DRS leading to inaccurate predictions of *T*. By integrating a novel, hyperspectral remote-sensing-based transformed version of CNDI to represent changes in leaf biochemistry, water content, and emissivity, we highlight the potential to improve thermal remote-sensing-based *T* modelling when drought and/or N stress occur simultaneously. Our results show that the future utilisation of combined thermal and hyperspectral technologies on regional or even global scales has the potential to markedly improve crop irrigation strategies and bolster future food security.

ACKNOWLEDGEMENTS

This work was supported by the UK Research and Innovation (UKRI) Future Leaders Fellowship scheme [MR/T01993X/1] and The Institute of Sustainable Food at the University of Sheffield. Open Access funding enabled and organized by Projekt DEAL.

CONFLICT OF INTEREST STATEMENT

The authors declare no conflict of interest.

DATA AVAILABILITY STATEMENT

The data that support the findings of this study are available from the corresponding author upon reasonable request.

ORCID

Robert S. Caine http://orcid.org/0000-0002-6480-218X
Muhammad S. Khan http://orcid.org/0000-0003-0506-5180
Robert A. Brench http://orcid.org/0000-0003-1900-4012
Heather J. Walker http://orcid.org/0000-0002-6815-0465
Holly L. Croft http://orcid.org/0000-0002-1653-1071

REFERENCES

Anderson, M. & Kustas, W. (2008) Thermal remote sensing of drought and evapotranspiration. *Eos, Transactions American Geophysical Union*, 89(26), 233–234.

Araus, V., Swift, J., Alvarez, J.M., Henry, A. & Coruzzi, G.M. (2020) A balancing act: how plants integrate nitrogen and water signals. *Journal of Experimental Botany*, 71(15), 4442–4451.

Banerjee, B.P., Joshi, S., Thoday-Kennedy, E., Pasam, R.K., Tibbits, J., Hayden, M. et al. (2020) High-throughput phenotyping using digital and hyperspectral imaging-derived biomarkers for genotypic nitrogen response. *Journal of Experimental Botany*, 71(15), 4604–4615.

Bertolino, L.T., Caine, R.S. & Gray, J.E. (2019) Impact of stomatal density and morphology on water-use efficiency in a changing world. *Frontiers in Plant Science*, 10, 225.

Bhusal, N., Lee, M., Reum Han, A., Han, A. & Kim, H.S. (2020) Responses to drought stress in *Prunus sargentii* and *Larix kaempferi* seedlings using morphological and physiological parameters. *Forest Ecology and Management*, 465, 118099.

Blomqvist, L., Yates, L. & Brook, B.W. (2020) Drivers of increasing global crop production: a decomposition analysis. *Environmental Research Letters*, 15(9), 0940b6.

Buckley, T.N. (2019) How do stomata respond to water status? *New Phytologist*, 224(1), 21–36.

Burnett, A.C., Anderson, J., Davidson, K.J., Ely, K.S., Lamour, J., Li, Q. et al. (2021a) A best-practice guide to predicting plant traits from leaf-level hyperspectral data using partial least squares regression. *Journal of Experimental Botany*, 72(18), 6175–6189.

Burnett, A.C., Serbin, S.P., Davidson, K.J., Ely, K.S. & Rogers, A. (2021b) Detection of the metabolic response to drought stress using hyperspectral reflectance. *Journal of Experimental Botany*, 72(18), 6474–6489.

Caine, R.S., Harrison, E.L., Sloan, J., Flis, P.M., Fischer, S., Khan, M.S. et al. (2023) The influences of stomatal size and density on rice abiotic stress resilience. *New Phytologist*, 237(6), 2180–2195.

Caine, R.S., Yin, X., Sloan, J., Harrison, E.L., Mohammed, U., Fulton, T. et al. (2019) Rice with reduced stomatal density conserves water and has improved drought tolerance under future climate conditions. *New Phytologist*, 221(1), 371–384.

Cao, X., Shen, Q., Shang, C., Yang, H., Liu, L. & Cheng, J. (2019) Determinants of shoot biomass production in mulberry: combined selection with leaf morphological and physiological traits. *Plants*, 8(5), 118.

Cao, Z., Wang, Q. & Zheng, C. (2015) Best hyperspectral indices for tracing leaf water status as determined from leaf dehydration experiments. *Ecological Indicators*, 54, 96–107.

Carter, G.A. (1993) Responses of leaf spectral reflectance to plant stress. *American Journal of Botany*, 80(3), 239–243.

Caturegli, L., Matteoli, S., Gaetani, M., Grossi, N., Magni, S., Minelli, A. et al. (2020) Effects of water stress on spectral reflectance of bermudagrass. *Scientific Reports*, 10(1), 15055.

Chen, J.M. & Liu, J. (2020) Evolution of evapotranspiration models using thermal and shortwave remote sensing data. *Remote Sensing of Environment*, 237, 111594.

Cotrozzi, L., Peron, R., Tuinstra, M.R., Mickelbart, M.V. & Couture, J.J. (2020) Spectral phenotyping of physiological and anatomical leaf traits related with maize water status. *Plant Physiology*, 184(3), 1363–1377.

Croft, H., Chen, J.M., Luo, X., Bartlett, P., Chen, B. & Staebler, R.M. (2017) Leaf chlorophyll content as a proxy for leaf photosynthetic capacity. *Global Change Biology*, 23(9), 3513–3524.

Croft, H., Chen, J.M. & Zhang, Y. (2014) The applicability of empirical vegetation indices for determining leaf chlorophyll content over different leaf and canopy structures. *Ecological Complexity*, 17, 119–130.

Curran, P.J., Dungan, J.L. & Gholz, H.L. (1990) Exploring the relationship between reflectance red edge and chlorophyll content in slash pine. *Tree Physiology*, 7(1_2_3_4), 33–48.

Dash, J. & Curran, P.J. (2007) Evaluation of the MERIS terrestrial chlorophyll index (MTCI). *Advances in Space Research*, 39(1), 100–104.

Du, Y.L., Wang, Z.Y., Fan, J.W., Turner, N.C., Wang, T. & Li, F.M. (2012) β-Aminobutyric acid increases abscisic acid accumulation and desiccation tolerance and decreases water use but fails to improve grain yield in two spring wheat cultivars under soil drying. *Journal of Experimental Botany*, 63(13), 4849–4860.

Duursma, R.A. (2015) Plantecophys—an R package for analysing and modelling leaf gas exchange data. *PLoS One*, 10(11), e0143346.

Evans, J.R. & Clarke, V.C. (2019) The nitrogen cost of photosynthesis. *Journal of Experimental Botany*, 70(1), 7–15.

Field, K.J., Rimington, W.R., Bidartondo, M.I., Allinson, K.E., Beerling, D.J., Cameron, D.D. et al. (2016) Functional analysis of liverworts in dual symbiosis with Glomeromycota and Mucoromycotina fungi under a simulated Palaeozoic CO_2 decline. *The ISME Journal*, 10(6), 1514–1526.

Franks, P.J. & Beerling, D.J. (2009) Maximum leaf conductance driven by CO_2 effects on stomatal size and density over geologic time. *Proceedings of the National Academy of Sciences*, 106(25), 10343–10347.

Franks, P.J., Leitch, I.J., Ruszala, E.M., Hetherington, A.M. & Beerling, D.J. (2012) Physiological framework for adaptation of stomata to CO_2 from glacial to future concentrations. *Philosophical Transactions of the Royal Society, B: Biological Sciences*, 367(1588), 537–546.

Gausman, H.W. & Allen, W.A. (1973) Optical parameters of leaves of 30 plant species. *Plant Physiology*, 52(1), 57–62.

Gerhards, M., Rock, G., Schlerf, M. & Udelhoven, T. (2016) Water stress detection in potato plants using leaf temperature, emissivity, and reflectance. *International Journal of Applied Earth Observation and Geoinformation*, 53, 27–39.

Guehl, J.-M., Fort, C. & Ferhi, A. (1995) Differential response of leaf conductance, carbon isotope discrimination and water-use efficiency to nitrogen deficiency in maritime pine and pedunculate oak plants. *New Phytologist*, 131(2), 149–157.

Guilioni, L., Jones, H.G., Leinonen, I. & Lhomme, J.P. (2008) On the relationships between stomatal resistance and leaf temperatures in thermography. *Agricultural and Forest Meteorology*, 148(11), 1908–1912.

Gupta, A., Rico-Medina, A. & Caño-Delgado, A.I. (2020) The physiology of plant responses to drought. *Science*, 368(6488), 266–269.

Hatfield, J.L. & Dold, C. (2019) Water-use efficiency: advances and challenges in a changing climate. *Frontiers in Plant Science*, 10, 103.

Haworth, M., Marino, G., Materassi, A., Raschi, A., Scutt, C.P. & Centritto, M. (2023) The functional significance of the stomatal size to density relationship: interaction with atmospheric [CO_2)] and role in plant physiological behaviour. *Science of the Total Environment*, 863, 160908.

Van Herwaarden, A.F., Angus, J.F., Richards, R.A. & Farquhar, G.D. (1998) 'Haying-off', the negative grain yield response of dryland wheat to nitrogen fertiliser II. Carbohydrate and protein dynamics. *Australian Journal of Agricultural Research*, 49(7), 1083–1094.

Huang, S., Tang, L., Hupy, J.P., Wang, Y. & Shao, G. (2021) Correction to: commentary review on the use of normalized difference vegetation index (NDVI) in the era of popular remote sensing. *Journal of Forestry Research*, 32(6), 2719.

Jones, H.G. (2002) Use of infrared thermography for monitoring stomatal closure in the field: application to grapevine. *Journal of Experimental Botany*, 53(378), 2249–2260.

Jones, H.G. (2013) *Plants and microclimate: a quantitative approach to environmental plant physiology*. Cambridge: Cambridge University Press.

Jones, H.G., Hutchinson, P.A., May, T., Jamali, H. & Deery, D.M. (2018) A practical method using a network of fixed infrared sensors for estimating crop canopy conductance and evaporation rate. *Biosystems Engineering*, 165, 59–69.

Katimbo, A., Rudnick, D.R., DeJonge, K.C., Lo, T.H., Qiao, X., Franz, T.E. et al. (2022) Crop water stress index computation approaches and their sensitivity to soil water dynamics. *Agricultural Water Management*, 266, 107575.

Kubar, M.S., Wang, C., Noor, R.S., Feng, M., Yang, W., Kubar, K.A. et al. (2022) Nitrogen fertilizer application rates and ratios promote the biochemical and physiological attributes of winter wheat. *Frontiers in Plant Science*, 13.

Kunrath, T.R., Lemaire, G., Teixeira, E., Brown, H.E., Ciampitti, I.A. & Sadras, V.O. (2020) Allometric relationships between nitrogen uptake and transpiration to untangle interactions between nitrogen supply and drought in maize and sorghum. *European Journal of Agronomy*, 120, 126145.

Leinonen, I., Grant, O.M., Tagliavia, C.P., Chaves, M.M. & Jones, H.G. (2006) Estimating stomatal conductance with thermal imagery. *Plant, Cell & Environment*, 29(8), 1508–1518.

Li, B., Xu, X., Zhang, L., Han, J., Bian, C., Li, G. et al. (2020) Above-ground biomass estimation and yield prediction in potato by using UAV-based RGB and hyperspectral imaging. *ISPRS Journal of Photogrammetry and Remote Sensing*, 162, 161–172.

Li, F., Miao, Y., Feng, G., Yuan, F., Yue, S., Gao, X. et al. (2014) Improving estimation of summer maize nitrogen status with red edge-based spectral vegetation indices. *Field Crops Research*, 157, 111–123.

Liu, H., Bruning, B., Garnett, T. & Berger, B. (2020) Hyperspectral imaging and 3D technologies for plant phenotyping: from satellite to close-range sensing. *Computers and Electronics in Agriculture*, 175, 105621.

Liu, L., Yang, X., Zhou, H., Liu, S., Zhou, L., Li, X. et al. (2018) Evaluating the utility of solar-induced chlorophyll fluorescence for drought monitoring by comparison with NDVI derived from wheat canopy. *Science of the Total Environment*, 625, 1208–1217.

Liu, Z. & Dickmann, D.I. (1996) Effects of water and nitrogen interaction on net photosynthesis, stomatal conductance, and water-use efficiency in two hybrid poplar clones. *Physiologia Plantarum*, 97(3), 507–512.

López-Serrano, M.J., Velasco-Muñoz, J.F., Aznar-Sánchez, J.A. & Román-Sánchez, I.M. (2020) Sustainable use of wastewater in agriculture: a bibliometric analysis of worldwide research. *Sustainability*, 12, 8948. Available from: https://doi.org/10.3390/su12218948

Matimati, I., Verboom, G.A. & Cramer, M.D. (2014) Nitrogen regulation of transpiration controls mass-flow acquisition of nutrients. *Journal of Experimental Botany*, 65(1), 159–168.

Meireles, J.E., Schweiger, A.K. & Cavender-Bares, J.M. (2017) *spectrolab: class and methods for hyperspectral data*. R package version 0.0. 2.

Mengel, K., Hütsch, B. & Kane, Y. (2006) Nitrogen fertilizer application rates on cereal crops according to available mineral and organic soil nitrogen. *European Journal of Agronomy*, 24(4), 343–348.

Mertens, S., Verbraeken, L., Sprenger, H., Demuynck, K., Maleux, K., Cannoot, B. et al. (2021) Proximal hyperspectral imaging detects diurnal and drought-induced changes in maize physiology. *Frontiers in Plant Science*, 12, 640914.

Mohd Asaari, M.S., Mertens, S., Verbraeken, L., Dhondt, S., Inzé, D., Bikram, K. et al. (2022) Non-destructive analysis of plant physiological traits using hyperspectral imaging: a case study on drought stress. *Computers and Electronics in Agriculture*, 195, 106806.

Monteith, J. & Unsworth, M. (2013) *Principles of environmental physics: plants, animals, and the atmosphere*. Academic Press.

Mu, X. & Chen, Y. (2021) The physiological response of photosynthesis to nitrogen deficiency. *Plant Physiology and Biochemistry*, 158, 76–82.

Oliveira, R.A., Näsi, R., Korhonen, P., Mustonen, A., Niemeläinen, O., Koivumäki, N. et al. (2024) High-precision estimation of grass quality and quantity using UAS-based VNIR and SWIR hyperspectral cameras and machine learning. *Precision Agriculture*, 25(1), 186–220.

Ookawa, T., Naruoka, Y., Sayama, A. & Hirasawa, T. (2004) Cytokinin effects on ribulose-1,5-bisphosphate carboxylase/oxygenase and nitrogen partitioning in rice during ripening. *Crop Science*, 44(6), 2107–2115.

Page, G.F.M., Liénard, J.F., Pruett, M.J. & Moffett, K.B. (2018) Spatio-temporal dynamics of leaf transpiration quantified with time-series thermal imaging. *Agricultural and Forest Meteorology*, 256-257, 304–314.

Peñuelas, J., Filella, I., Biel, C., Serrano, L. & Savé, R. (1993) The reflectance at the 950–970 nm region as an indicator of plant water status. *International Journal of Remote Sensing*, 14(10), 1887–1905.

Peron-Danaher, R., Cotrozzi, L., Masjedi, A., Enders, L.S., Krupke, C.H., Mickelbart, M.V. et al. (2023) Drought stress affects spectral separation of maize infested by western corn rootworm. *Agronomy*, 13, 2562. Available from: https://doi.org/10.3390/agronomy13102562

Plett, D.C., Ranathunge, K., Melino, V.J., Kuya, N., Uga, Y. & Kronzucker, H.J. (2020) The intersection of nitrogen nutrition and water use in plants: new paths toward improved crop productivity. *Journal of Experimental Botany*, 71(15), 4452–4468.

R Team. (2021) *R: a language and environment for statistical computing*, Vienna, Austria: R Foundation for Statistical Computing 2012.

Saari, H., Akujärvi, A., Holmlund, C., Ojanen, H., Kaivosoja, J., Nissinen, A. et al. (2017) Visible, very near IR and short wave IR hyperspectral drone imaging system for agriculture and natural water applications. *The International Archives of the Photogrammetry, Remote Sensing and Spatial Information Sciences*, XLII-3/W3, 165–170.

Sage, R.F., Pearcy, R.W. & Seemann, J.R. (1987) The nitrogen use efficiency of C(3) and C(4) plants: III. Leaf nitrogen effects on the activity of carboxylating enzymes in *Chenopodium album* (L.) and *Amaranthus retroflexus* (L.). *Plant Physiology*, 85(2), 355–359.

Sarić, R., Nguyen, V.D., Burge, T., Berkowitz, O., Trtílek, M., Whelan, J. et al. (2022) Applications of hyperspectral imaging in plant phenotyping. *Trends in Plant Science*, 27(3), 301–315.

Seelig, H.D., Hoehn, A., Stodieck, L.S., Klaus, D.M., Adams Iii, W.W. & Emery, W.J. (2008) The assessment of leaf water content using leaf reflectance ratios in the visible, near-, and short-wave-infrared. *International Journal of Remote Sensing*, 29(13), 3701–3713.

Seibt, U., Rajabi, A., Griffiths, H. & Berry, J.A. (2008) Carbon isotopes and water use efficiency: sense and sensitivity. *Oecologia*, 155(3), 441–454.

Shimshi, D. (1970) The effect of nitrogen supply on transpiration and stomatal behaviour of beans (*Phaseolus vulgaris* L.). *New Phytologist*, 69(2), 405–412.

Shiratsuchi, L., Ferguson, R., Shanahan, J., Adamchuk, V., Rundquist, D., Marx, D. et al. (2011) Water and nitrogen effects on active canopy sensor vegetation indices. *Agronomy Journal*, 103(6), 1815–1826.

Sun, H., Feng, M., Yang, W., Bi, R., Sun, J., Zhao, C. et al. (2022) Monitoring leaf nitrogen accumulation with optimized spectral index in winter wheat under different irrigation regimes. *Frontiers in Plant Science*, 13, 913240.

Topcu, S., Kirda, C., Dasgan, Y., Kaman, H., Cetin, M., Yazici, A. et al. (2007) Yield response and N-fertiliser recovery of tomato grown under deficit irrigation. *European Journal of Agronomy*, 26(1), 64–70.

Verlinden, M.S., Fichot, R., Broeckx, L.S., Vanholme, B., Boerjan, W. & Ceulemans, R. (2015) Carbon isotope compositions (δ13C) of leaf, wood and holocellulose differ among genotypes of poplar and between previous land uses in a short-rotation biomass plantation. *Plant, Cell & Environment*, 38(1), 144–156.

Vialet-Chabrand, S. & Lawson, T. (2019) Dynamic leaf energy balance: deriving stomatal conductance from thermal imaging in a dynamic environment. *Journal of Experimental Botany*, 70(10), 2839–2855.

Viña, A., Gitelson, A.A., Nguy-Robertson, A.L. & Peng, Y. (2011) Comparison of different vegetation indices for the remote assessment of green leaf area index of crops. *Remote Sensing of Environment*, 115(12), 3468–3478.

Wall, S., Vialet-Chabrand, S., Davey, P., Van Rie, J., Galle, A., Cockram, J. et al. (2022) Stomata on the abaxial and adaxial leaf surfaces contribute differently to leaf gas exchange and photosynthesis in wheat. *New Phytologist*, 235(5), 1743–1756.

Wang, Z., Li, G., Sun, H., Ma, L., Guo, Y., Zhao, Z. et al. (2018) Effects of drought stress on photosynthesis and photosynthetic electron transport chain in young apple tree leaves. *Biology Open*, 7(11), bio035279.

Wellburn, A.R. (1994) The spectral determination of chlorophylls a and b, as well as total carotenoids, using various solvents with spectrophotometers of different resolution. *Journal of Plant Physiology*, 144(3), 307–313.

Witten, D. & James, G. (2013) *An introduction to statistical learning with applications in R*. springer publication

Woo, N.S., Badger, M.R. & Pogson, B.J. (2008) A rapid, non-invasive procedure for quantitative assessment of drought survival using chlorophyll fluorescence. *Plant Methods*, 4(1), 27.

Xu, R., Tian, H., Pan, S., Prior, S.A., Feng, Y. & Dangal, S.R.S. (2020) Global N2O emissions from cropland driven by nitrogen addition and environmental factors: comparison and uncertainty analysis. *Global Biogeochemical Cycles*, 34(12), e2020GB006698.

Yang, M., Hassan, M.A., Xu, K., Zheng, C., Rasheed, A., Zhang, Y. et al. (2020) Assessment of water and nitrogen use efficiencies through UAV-based multispectral phenotyping in winter wheat. *Frontiers in Plant Science*, 11, 927.

Yang, X., Lu, M., Wang, Y., Wang, Y., Liu, Z. & Chen, S. (2021) Response mechanism of plants to drought stress. *Horticulturae*, 7, 50. Available from: https://doi.org/10.3390/horticulturae7030050

Yu, G.-R. (2000) A proposal for universal formulas for estimating leaf water status of herbaceous and woody plants based on spectral reflectance properties. *Plant and Soil*, 227(1), 47–58.

Zotarelli, L., Dukes, M.D., Romero, C.C., Migliaccio, K.W. & Morgan, K.T. (2010) Step by step calculation of the Penman-Monteith evapotranspiration (FAO-56 method). *Institute of Food and Agricultural Sciences, University of Florida*, 8.

SUPPORTING INFORMATION

Additional supporting information can be found online in the Supporting Information section at the end of this article.

How to cite this article: Caine, R.S., Khan, M.S., Brench, R.A., Walker, H.J. & Croft, H.L. (2024) Inside-out: synergising leaf biochemical traits with stomatal-regulated water fluxes to enhance transpiration modelling during abiotic stress. *Plant, Cell & Environment*, 1–20. https://doi.org/10.1111/pce.14892